Quantification of single molecule glycan-mannose receptor binding kinetics on myeloid cells reveals high subcellular binding heterogeneity

Kas Steuten[1], Johannes J.A. Bakker[1], Ward Doelman[1], Diana Torres-García[1], Roger Riera[2], Lorenzo Albertazzi[2], Sander I. van Kasteren[1]*

Department of Chemical Biology and Immunology, Leiden Institute of Chemistry, Leiden University, Leiden, the Netherlands[1]

Department of Biomedical Engineering and Institute for Complex Molecular Systems, Eindhoven University of Technology, Eindhoven, the Netherlands[2]

*Correspondence: s.i.van.kasteren@chem.leidenuniv.nl

Keywords

Live-Cell Kinetics, Single-molecule kinetics, Mannose Receptor, Cross-Presentation, Glyco-PAINT

Abstract

Extracting single-molecule lectin binding kinetics from primary cells has not been possible to date. Here, we present **Glyco-PAINT-APP** (Automated Processing Pipeline), an automated method that enables the extraction of subcellular glycan interaction kinetics using a Points Accumulation for Imaging in Nano-Topography (PAINT)-based approach. This approach leverages an algorithm for precise, high-throughput subcellular analysis of glycan binding dynamics, facilitating the exploration of functional correlations between glycoform binding patterns and immune cell polarization. Using synthetic glycans and glycosylated antigens, we demonstrate the ability of the technique to automatically correlate glycan binding parameters in subregions of dendritic cell membranes with increased uptake and cross-presentation efficiency of these antigens. Additionally, we show how the method can uncover subtle differences in glycan binding preferences between resting and polarized macrophages. Taken together, Glyco-PAINT-

28 APP has the potential to enable new insights into the cell-intrinsic heterogeneity of
29 glycan-structure-activity relationships in immune cells.

30 **Introduction**

31 Myeloid immune cells such as dendritic cells and macrophages are key sentinels of the
32 immune system. They sense the presence of microbial species or altered self through
33 pattern recognition receptors (PRRs), which in turn can trigger innate and adaptive
34 immune responses. One important family of PRRs are the carbohydrate-binding proteins
35 of the C-type lectin receptor family (CLRs).[1,2] CLR ligation can induce various immune
36 functions, including endocytosis, polarization, cytokine secretion, cell adhesion, and
37 motility, which can subsequently trigger downstream immune responses.[1,3]

38 The signalling pathways leading to these biological outcomes are intricate and finely
39 tuned, which complicates the study of how the emit signals upon ligand recognition,
40 particularly in their native environment on the cell surface. This complexity arises from a
41 variety of factors: binding of the receptors to ligands is weak and often multivalent,
42 multiple receptors have overlapping specificities, and the surface expression patterns of
43 CLRs can be highly dynamic. Myeloid cells express a diverse array of CLRs for sensing
44 aberrant glycosylation. These can exists as monomers, multimers, and even form
45 heterodimeric complexes[4,5]. Various factors, such as the polarization state of the cell
46 modulates the expression levels of these lectins, as well as the cycling of these lectins
47 between the surface and intracellular storage pools.[6,7] The resulting dynamic and
48 heterogeneous surface expression leads to significant variability in receptor-ligand
49 interactions.

50 To complicate matters further, myeloid cells also present a repertoire of glycans that
51 serve as ligands for their lectins that can modulate signalling pathways through ligand
52 competition, and receptor clustering. Polarization also influences the expression of
53 these cis-ligands, adding yet another layer of complexity.[8,9] The final complicating factor
54 in CLR-binding and signalling is that the affinities of CTLs for their ligands are weak (K_D in
55 μM to mM range)[10], which complicates the detection and precise study of these
56 interactions. Together with the intrinsic chemical complexity of glycan ligands, these
57 factors have made it exceedingly difficult to establish clear relationships between glycan

58 binding properties and lectin function, particularly as studying these lectins out of their
59 native context also removes these modulating factors.

60 We have recently reported a technique for quantifying carbohydrate-lectin binding
61 kinetics on cell lines called Glyco-PAINT.[11] Glyco-PAINT exploits the transient interaction
62 between fluorescently-labelled sugars and their receptors to generate single molecule
63 binding events[11], analogous to those induced by the mismatches of DNA-strands in
64 conventional Points Accumulation for Imaging in Nanoscale Topography (DNA-PAINT)-
65 imaging.[12] Accumulation of these binding events over time allows for a complete
66 mapping of receptor-ligand interactions on the cell surface and subsequent
67 derivatization of kinetic parameters such as on-rate, off-rate and diffusion coefficients on
68 a per-cell basis derived from single-molecule binding information.

69 We envisaged that Glyco-PAINT could be a powerful technique to unravel the complexity
70 of myeloid lectin binding, as the single molecule as well as the live cell aspects of the
71 technique are ideal for studying these capricious receptors within their native
72 environment on the myeloid cell surface. However, three major hurdles needed to be
73 overcome to achieve this. The first is that Glyco-PAINT had only been demonstrated in an
74 over-expression system. Second, the Glyco-PAINT processing pipeline could only be
75 used to obtain the binding parameters averaged over the surface of a whole cell, which
76 we hypothesized to be insufficient, due to the microheterogeneity of receptor expression
77 on primary cells. The final problem relates to the probes: the Glyco-PAINT reagents
78 consist of a carbohydrate cluster directly attached to a fluorophore, which minimises the
79 downstream immunological evaluation of receptor biology, therefore precluding the
80 correlation of binding to biological function.

81 One receptor which is archetypal in its and biological complexity is the mannose receptor
82 (CD206, MR). This lectin is expressed on cells of the myeloid lineage[13–15], where it carries
83 out multiple functions: as an endocytic receptor to clear glycoproteins, as a phagocytic
84 receptor binding to, and internalizing, glycosylated particles for clearance and antigen
85 presentation[16–18], and as a mediator of inflammatory signalling by inducing M2
86 polarization of macrophages and inducing T cell tolerance.[19,20] How the MR translates
87 ligand recognition to all these functions remains unknown. Structurally, the MR contains
88 multiple functional domains, including an N-terminal cysteine-rich domain capable of

89 binding sulphated glycans (that can inhibit receptor function[21]), a fibronectin-like domain
90 capable of binding collagen peptides[22,23], and eight C-type lectin domains (CTLs), of
91 which only CTL4 and CTL5 exhibit functional calcium-dependent binding of neutral
92 sugars.[24] These domains are further modulated by glycosylation at seven N-linked sites,
93 influencing receptor binding properties.[25] Moreover, the intracellular tail lacks classical
94 signalling motifs [6,16], though recent evidence suggests phosphorylation and diaromatic
95 motifs may facilitate endosomal sorting and signalling.[26–28]

96 Despite its biological complexity, MR has been under heavy investigation as vaccine
97 receptor. Ligation of the MR was shown to lead to the enhanced cross-presentation (and
98 thus cytotoxic CD8 T-cell activation) of glycoprotein antigens, which can be employed to
99 enhance the anti-cancer and anti-viral properties of therapeutic vaccines.[29] However,
100 further pursuit of this phenomenon has led to conflicting results.[30–38] No studies have yet
101 managed to correlate the binding of ligands to the MR to downstream biology (i.e., uptake
102 and/or cross-presentation). Studies using bulk methods, such as surface plasmon
103 resonance (SPR), failed to correlate binding affinities with uptake or cross-presentation,
104 highlighting the need for methodologies capable of quantifying receptor-ligand kinetics
105 in the native cellular context.[11,31]

106 Here, we present the redevelopment of Glyco-PAINT, such that we can obtain binding
107 parameters of glycans to the MR on myeloid cells. We have developed a new analysis
108 algorithm to independently process large volumes of Glyco-PAINT recordings of glycan
109 binding events to primary immune cells in such a way that binding event concentration,
110 dwell times, diffusion coefficients and displacement can be determined for the highly
111 heterogeneous and disperse binding observed across the cell basal membrane of
112 dendritic cells and macrophages. We have dubbed this method "Glyco-PAINT-
113 Automated Processing Pipeline" (Glyco-PAINT-APP). In addition, we developed a new
114 probe library containing a pendant cross-presentable epitope that allowed us to quantify
115 lectin binding kinetics, uptake, and cross-presentation of the same construct.
116 Correlating the binding kinetics to uptake and cross-presentation biology yielded
117 surprising findings. The first of these was, as described above, that binding events are not
118 homogeneously distributed across the DC or macrophage membrane.

119 In addition – using the novel segmentation approach – we found a strong negative
120 correlation (Pearson's R: 0.90) between the cell surface mobility of ligands to subsequent
121 endocytosis by the DC. In contrast, cross-presentation of mannosylated antigens
122 showed a strong positive correlation to the residence time on the DC (Pearson's R: 0.94)
123 independent of the amount of surface mobility. In a second application of the approach,
124 we could also quantify changes in mannoside binding during the macrophage
125 polarisation trajectory from M0 to M2, but not M1.
126
127 **Results**
128 *Quantifying glycan-lectin binding on primary DC*

129 Our first aim was to determine whether the Glyco-PAINT methodology could be used to
130 study binding events on the surface of primary bone-marrow derived mouse dendritic
131 cells (BMDCs).[39] Unlike the overexpression system used previously, BMDCs suffer from
132 heterogeneous and dynamic receptor expression, broad lectin repertoires, and structural
133 features such as tight focal adhesions and podosomes that may exclude binding events
134 from the TIRF plane.[40,41]

135 Preliminary attempts to quantify binding kinetics of a labelled mannose glycan library on
136 BMDCs yielded a surprising result: whereas binding events could clearly be seen in the
137 Glyco-PAINT recordings (**Figure 1B** and **Figure S1A-D**) no significant differences were
138 observed between the probes for either the events $\mu m^{-2} sec^{-1}$ (a parameter that correlates
139 to k_{on*}[receptor concentration]), nor in the average ligand dwell time (**τ**, which is the
140 inverse of the off rate, or k_{off}^{-1}) (**Figure S1E-F**). Control experiments in CHO-MR cells did
141 show the binding behaviour as originally reported (**Figure 1A** and **Figure S2A-D** and
142 **Figure S2E, F** for quantification).

143 Interestingly, density maps did reveal a stark heterogeneity of binding events, both
144 between cells – with some cells devoid of binding events, and other showing large
145 numbers of events – but also between different regions of the basal membrane of a single
146 BMDC. Areas of high binding events were observed overlapping with brightfield-defined
147 cell outlines (**Figure 1B** green areas and **Figure S1A-D**). However, large areas of the cell
148 basal membrane were also devoid of any binding event density (**Figure 1B** red areas and
149 **Figure S1A-D**). Areas outside the brightfield-defined cell surface appeared to be also

engaging in binding events (**Figure 1B,** blue areas), suggesting the presence of receptors on ultrathin dendritic protrusions. This heterogeneity was not observed for CHO-MR cells (**Figure 1A**, green areas and **Figure S2**).

These observations meant that the fundamental assumption underpinning the Glyco-PAINT method – that the receptor concentration [R] is homogeneous over the whole basal membrane – was incorrect. This in turn implicates that the per-cell relative on-rate was an irrelevant parameter for the study of primary cells. The off-rates too are averaged on a per-cell basis as they are integrated over the complete area only a subsection contains binding-enabled lectins. Taken together, the observed highly heterogeneous binding event distribution, therefore renders the assumption of a constant and homogeneous receptor concentration incorrect and calls for a more dynamic surface area definition as to obtain meaningful quantification of kinetic parameters.

Glyco-PAINT-APP

To address the heterogeneity observed on BMDC surfaces, we developed the Glyco-PAINT-Automated Processing Pipeline (Glyco-PAINT-APP). Instead of using the whole cell as the averaging unit, subcellular regions are selected. This allows precise quantification of glycan binding kinetics within localized areas. This new workflow has fully automated every step of the Glyco-PAINT analysis method, accelerating analysis speed. The Glyco-PAINT-APP is schematically outlined in **Figure 1C** (and described in full detail in the **Supplementary Manual**).

Glyco-PAINT-APP starts with subjecting sets of microscope recordings representing individual Glyco-PAINT experiments to single particle tracking analysis (see also **Supplementary Video 1**). This yields output files containing spatial information belonging to each spot and the resulting tracks formed by connecting closely linked spots through multiple consecutive frames. We then apply a new processing algorithm to these data where, instead of manual cell definition by ROI drawing, a raster of squares (typically 20x20 squares per field of view) is laid over the image. Kinetic information is then averaged per square, rather than per cell. Quality control parameters such as the *Density Ratio*, *Maximum Variability* and *Connectivity* can be retrieved per square to accurately discriminate signal from background. *Density Ratio* is a measure for signal-to-background (by setting background levels as the 10% squares with lowest event density

181 but containing at least one event), *Maximum Variability* is a heterogeneity score for event
182 distribution within a square and *Connectivity* is a measure for squares being surrounded
183 by adjacent squares or not. Further selection takes place via statistical parameters such
184 as the *R Squared* value that relates to the quality of the one-phase exponential decay fit
185 or minimum number of binding events (see **Supplementary Manual** for a detailed
186 description of quality control parameters). The interactive tuning of these parameters
187 using the *Select Squares* window together with visual feedback from the *Recording*
188 *Viewer* (**Figure 1C** and **Supplementary Video 2**) where the tracking overlay with grids and
189 brightfield image are displayed side by side allows for user-informed data curation.
190 Kinetic parameters including glycan on- and off-rates, diffusion coefficients, speed,
191 displacement and maximum, average, or total binding event duration can be displayed
192 for each square per recording using the heatmap toggle function in the *Recording Viewer*
193 (**Figure 1C**). The *Compile Project* built-in modality can integrate kinetic data from
194 multiple recordings obtained from multiple biological replicates within a single project
195 and can generate a merged output file to which statistical analysis can be applied with
196 scientific graphing software of choice (R Studio[43], GraphPad Prism, etc.), yielding a
197 suitable method for the study of biological systems with the required biological
198 replicates.

199 *Subcellular analysis of immune cell lectin binding*

200 We then applied Glyco-PAINT-APP to the profiling of glycan binding events on DC. This
201 required us to first optimize the grid size. For this we used the complete dataset of
202 mannose ligands binding to BMDC, which consists of approximately 300 different
203 recordings (each of standard 81 x 81 μm^2, 512 x 512 pixels, and 2000 frames at 20 fps).
204 Our analysis demonstrated that 20 squares per axis provided an optimal balance
205 between statistical quality, the number of binding events, and the minimization of
206 averaging artifacts (**Figure S5**). *R Squared* distribution remained in the 0.7-1 range for the
207 chosen grid size. Off-rates (**τ)** and density (rel. k_{on}) values diverged, reflecting enhanced
208 sensitivity for measurement of inherently heterogeneous systems.

209 With this new analysis pipeline in hand, we set out to reprocess the recordings of the
210 mannose probe library on primary DCs for which the original Glyco-PAINT procedure had
211 not yielded any significant differences in binding between the different glycoforms. The

212 square-based analysis for DCs is displayed in **Figure 2** (for the same recordings as in
213 **Figure S1**) and extended in **Figure S3** for mono- and trimannosides **8**, **10**, **11** and **13**. From
214 **Figure 2B and F**, it can be seen that the new algorithm was able to independently
215 distinguish areas with binding event density from background using filtering based on
216 uniform parameters for the entire experiment. The added advantage of this approach is
217 that binding events that fell outside brightfield-invisible features of the DC, such as on
218 the dendrites that lend the cells their name, are now also included in the analysis. The
219 thus observed binding rates in different areas of the cell basal membrane can be
220 visualised as heatmaps in **Figure 2C, D** and **G, H**. The grid-based analysis by Glyco-
221 PAINT-APP even improves the effective selection of cell areas engaged in binding events
222 for mono- and trimannoside-based probe binding to CHO-MR (**Figure S4**), highlighting
223 the omnipresence of microheterogeneity even in overexpression systems. Taken
224 together, this method allows for precise analysis of glycan-lectin interactions on live
225 immune cells with intrinsically heterogenic expression avoiding the emergence of
226 averaging artefacts as in the original Glyco-PAINT analysis. In addition, some interesting
227 parameters began to emerge. For example, a discrepancy between areas of high number
228 of binding events (i.e., high $[R]*k_{on}$; **Figure 2C, G**) and areas with long average duration of
229 binding (**τ**, k_{off}^{-1}, **Figure 2D, H**) within the same cell.

230 *Uptake and antigen presentation of SLP glycoforms*

231 We next wanted to determine whether any of the on-cell kinetic parameters could prove
232 predictive for some of the previously reported roles (see introduction) of the MR and
233 related CLRs on BMDCs. We therefore designed Synthetic Long Peptide (SLP) versions of
234 the fluorophore-labelled mannose clusters that also contained the model cross-
235 presentable epitope $Ovalbumin_{247-264}$ (OVA SLP)[44], as it has been hypothesized that
236 different glycoforms of these SLPs show different cross-presentation behaviour.[34,45] This
237 additional feature would allow us to not only monitor the various binding parameters (by
238 Glyco-PAINT-APP), but also uptake (by flow cytometry) and antigen cross-presentation
239 (using the cognate OT-I T-cell), thereby having readouts for these three aspects of MR
240 biology from a single probe.

241 The constructs were synthesized using in-line solid-phase peptide synthesis of the
242 peptide antigen and an oligo-azidolysine (6-azidonorleucine) cluster, followed by on-

243 resin modification with fluorophore. Copper-catalysed azide-alkyne cycloaddition
244 (CuAAC)-mediated[46,47] coupling of the mannose glycans to the azidolysine clusters in
245 solution yielded the target glycosylated SLPs. This resulted in mono-, bi- and hexavalent
246 versions of mono- (**1-3**) or trimannosylated (**4-6**) SLPs and a non-glycosylated control
247 molecule (**7**) that are displayed in **Figure 3A** (synthetic procedures and characterization
248 can be found in the supplementary information and **Figure S6**). These glycan motifs span
249 a K_D range for MR-binding from 3 μM to more than 100 μM (based on SPR studies[11,31]),
250 thereby enabling investigation of glycan-structure-binding-activity relationships over a
251 large affinity range.

252 To verify the absence of artefacts resulting from the SLP antigenic cargo on kinetics we
253 compared the median on- and off-rates of OVA SLP **1-6** to glycoclusters **8-13** on CHO-MR
254 cells and plotted the correlation between the two in **Figure 3B, C**. Neither extension of
255 the peptide core, nor the change of the fluorophore from ATTO655 to sulfo-Cy5
256 significantly affected k_{off}. A decrease in the median number of binding events per square
257 was detected for the glycan SLPs with respect to the glycans **8-13**, potentially originating
258 from modestly altered physical-chemical properties of the peptide cargo.

259 The binding parameters of these glycosylated SLPs to live DC were then determined using
260 the Glyco-PAINT-APP. To prevent the termination of binding events by endocytosis –
261 which is one of the biological functions resulting from MR-ligation – we also performed
262 kinetic measurements after 30 minutes treatment of the cells with Cytochalasin D
263 (CytD), an inhibitor of actin polymerization.[48,49] This inhibitor is known to inhibit many
264 endocytic pathways that depend on F-actin filament polymerisation. We obtained off-
265 rates and diffusion coefficients per square for **1-7** after CytD addition (**Figure 4A, B**, and
266 **Table S1**) and compared glycoform-specific trends to those of non-CytD-treated cells.
267 On-rates, off-rates and diffusion coefficients were significantly increased for all
268 glycosylated probes **1-6** after DC and CHO-MR treatment with Cytochalasin D (**Figure 4A,**
269 **B** and **Table S1**, and **Figure S7)** but not for the non-glycosylated control antigen **7**.
270 Confirming the interactions for these probes being glycan-lectin-mediated, particularly
271 those that depend on actin polymerization and rearrangement of the cytoskeleton for
272 endocytosis.

273 Next, the uptake of these SLPs was measured by incubating BMDCs with SLP **1-7** for 1h,
274 followed by quantification of the sCy5 signal by flow cytometry. The histograms in **Figure**
275 **4C** show that a specific subpopulation of MR^+CD11c^+ DCs (**Figure S8B**, for MR co-
276 staining) are mostly engaged in this MR-mediated uptake (**Figure S8A,** for competition
277 with MR ligand mannan), highlighting the intrinsic heterogeneity of these cells.
278 Quantification of this effect using phagocytic index (PI)[50] revealed a distinct glycoform-
279 specific profile with divalent trisaccharide-modified SLP **5** being most effectively taken
280 up in contrast to its hexavalent counterpart **6**. Uptake of the non-glycosylated control **7**
281 was below the limit of detection, emphasizing the glycan-mediated engagement of
282 endocytic lectins.

283 The cross-presentation efficiency of these glycosylated SLPs was tested next by pulsing
284 differentiated DCs, which were matured for 2 hours with TLR4 ligand MPLA, with 40 nM
285 SLP (which is in a similar concentration range as Glyco-PAINT binding studies, see **Figure**
286 **S8C, D** for different antigen dosages and quantification) for 2h followed by a 3-day
287 coculture with cognate CD8 T cells that were freshly isolated from OT-I mice. To our
288 surprise, non-mannosylated control **7** was most efficiently cross-presented whereas
289 SLPs decorated with mannosides of increasing complexity and valency **1-6** showed a
290 surprising decrease in T-cell activation/proliferation induction. Being aware of the
291 controversy around the precise role of the MR in antigen cross-presentation[33–36], we
292 verified next to antigen dose and DC origin (see **Figure S8F** for steady-state cross-
293 presentation of antigens in splenic DCs[34]), the effect of the timing of DC maturation and
294 found an identical pattern for all timepoints in agreement with the observed diminishing
295 effect of antigen mannosylation on T cell proliferation (**Figure S8E** and **G**).

296 Having observed this non-linear (**Figure S9**) and, to us at least, counter-intuitive
297 relationship between binding, the amounts of endocytosed antigen, and MHC-I-
298 restricted cross-presentation, we next determined whether any of the subcellular kinetic
299 parameters of SLP binding to DCs was predictive of either of these biological functions.
300 A correlation study was performed using the median values of the following 10 kinetic
301 parameters as derived by Glyco-PAINT-APP per analysed square: **τ** (ms), rel. k_{on}
302 (events·$sec^{-1}$$\mu m^{-2}$), total track duration (s), long track duration (10% longest, s), short
303 track duration (90% shortest, s), diffusion coefficient (nm^2sec^{-1}), speed ($\mu m \cdot s^{-1}$) and max.

304 speed ($\mu m \cdot s^{-1}$). In **Table S2** Pearson's R for the correlation between all these parameters
305 and the phagocytic index or cross-presentation efficiency of SLP **1-7** is listed. Notably,
306 glycan-SLP residence time (**τ**) on the DC surface was the best predictor for cross-
307 presentation, whereas high diffusion coefficients (and accordingly larger displacement
308 of the track) correlated with low uptake of the SLP (**Figure 4E, H**). These observations
309 imply a mechanism where binding events of long duration and high on-membrane
310 mobility are less likely to result in receptor-mediated endocytosis but more likely to enter
311 a cytosolic cross-presentation pathway. Taken together, the strong correlations between
312 on-cell kinetics and cellular functionality demonstrate the potential of the Glyco-PAINT-
313 APP to uncover functional glycan-structure-activity relationships.

314 *CLR dynamics in polarizing macrophages*

315 To further explore the utility of Glyco-PAINT-APP we studied the changes in carbohydrate
316 binding upon macrophage polarization. Certain pro- and anti-inflammatory stimuli are
317 known to affect absolute levels of the MR on the cell surface upon polarisation of the
318 macrophage from its 'naïve' M0-like state to either the inflamed M1-like or wound-healing
319 M2-like phenotype.[51] It is, however, not known whether this change in MR (and related
320 CLR)-levels also alters binding preferences of the macrophage. We attempted to
321 investigate this by quantifying the binding parameters of MR ligand hexatrimannoside **6**
322 to murine bone marrow-derived macrophages (BMDM) treated with either M1 inducing
323 (LPS and IFNy) or M2-inducing (IL-4) stimuli (**Figure 5A-C**). Quantification of the number
324 of binding events (rel. $[R]*k_{on}$) indicated that the number of **6**-binding receptors was
325 markedly increased upon M2-polarization (**Figure 5F**). When looking at the total binding
326 as quantified by the total track duration (number of events multiplied with their duration)
327 within a square, there appeared to be a vast increase upon M2 stimulation and slight
328 decrease for the M1 phenotype (**Figure 5G**). This suggests the emergence of a new
329 population of long duration binding events that are potentially the result of CLR
330 upregulation by M2 macrophages. Additionally, binding events in the M2 state exhibited
331 longer diffusion coefficients compared to the M1 or naïve states, indicating the presence
332 of a distinct subpopulation (**Figure 5D** and **H**). Taken together, these kinetic data suggest
333 a mechanism where CLR shuttling is enhanced in inflammatory M1 macrophages, while
334 cell surface dwell times are prolonged in the M2-like state.

335

336 **Discussion**

337 This paper describes the single-molecule quantification of glycan-lectin binding on
338 primary immune cells. Whilst quantification of glycan-lectin binding using glycan
339 arrays[52], SPR[53] or ELISA-based[54] technologies with immobilised ligands has yielded a
340 wealth of information related to binding preferences of individual lectins to glycans and
341 vice versa, it has never done so in the context of the living cell surface, where the
342 glycocalyx, other lectins and the constant movement of the membrane can affect glycan
343 binding. Glyco-PAINT-APP offers a significant technological advance that enables the
344 study of glycan-lectin binding in its native context. It is particularly potent, as it now
345 allows the quantification of binding of non-homogeneous distributions of binding events
346 on the cell surface. The method starts with PAINT recordings of glycan binding to
347 heterogeneous, semi-adherent, cell types and is able to extract kinetic information in the
348 form of off-rates, relative on-rates, diffusion coefficients, displacement and speed of the
349 receptor-ligand interaction in an unbiased and high-throughput manner whilst respecting
350 the subcellular variations typically associated with live cells of primary origin. We believe
351 that the Glyco-PAINT-APP can be of use to expand the information that can be obtained
352 from all PAINT-like technologies where increasingly attention is shifting to the use of
353 physiological ligands such as peptides, glycans and proteins as imaging probes beyond
354 the original DNA-PAINT method.[55–57] Furthermore, our approach could aid in fundamental
355 investigations into the dynamics of immune cell lectins of other families such as the
356 Siglecs. It could also be of use for structure-function or target-engagement studies of
357 other ligands that have a typical low affinity interaction with their receptors such as low-
358 affinity antibodies, peptides or TCR-pMHC interactions[58,59], or the other interactions
359 where (weak) binding affinities do not appear to correlate with function, such as the
360 recently reported anti-CD40 antibody library, where affinity reduction led to increased
361 receptor engagement.[60]

362 The second advance is that in this work, the live-cell kinetic parameters that were
363 obtained with the Glyco-PAINT-APP-approach could be correlated to receptor functions,
364 such as uptake and cross-presentation, which had been the subject of much controversy.
365 The wealth of binding and receptor-ligand information obtained by this approach – which

had previously thwarted correlation of bulk binding parameters to function - led us to identify key parameters of the interaction that could be predictive of uptake and cross-presentation behaviour: the presence of regions with very long ligand dwell times correlated with cross-presentation ability, and the lack of ligand movement of the receptor with internalisation. This – combined with the fact that uptake efficiency and cross presentation showed no correlation – suggests that multiple processes are likely taking place on the cell surface, either mediated by other lectins, or perhaps simply the micropinocytosis of which dendritic cells display a phenomenal rate: they can internalise their entire cell membrane in about half an hour, or the equivalent of a cell volume in an hour.[61,62] Watts and co-workers have shown macropinocytosis to be a key mechanism for inducing antigen cross-presentation.[63,64] We propose the hypothesis that the increased dwell time on the surface of a dendritic cell – either through receptor mediated interaction or through a-specific interactions – increases the chance of an antigen being internalised in a macropinosome. At the same time, the binding of a ligand to a clathrin-anchored MR increases its chance of internalisation into a non-cross presentation enabled vesicle. To precisely delineate the cell biology of these mechanisms, further studies using for example genetic knockouts of DC internalizing receptors are needed. This model, would however, explain some of the other reports of non-linear uptake-cross-presentation relationships for mannosylated SLPs[30–32] and potentially even for antibody-antigen conjugates.[65]

References

(1) Sousa, C. R. e; Yamasaki, S.; Brown, G. D. Myeloid C-Type Lectin Receptors in Innate Immune Recognition. *Immunity* **2024**, *57* (4), 700–717. https://doi.org/10.1016/j.immuni.2024.03.005.

(2) *Essentials of Glycobiology*, 4th ed.; Varki, A., Cummings, R. D., Esko, J. D., Stanley, P., Hart, G. W., Aebi, M., Mohnen, D., Kinoshita, T., Packer, N. H., Prestegard, J. H., Schnaar, R. L., Seeberger, P. H., Eds.; Cold Spring Harbor Laboratory Press: Cold Spring Harbor (NY), 2022.

(3) Marth, J. D.; Grewal, P. K. Mammalian Glycosylation in Immunity. *Nat Rev Immunol* **2008**, *8* (11), 874–887. https://doi.org/10.1038/nri2417.

(4) Tachado, S. D.; Zhang, J.; Zhu, J.; Patel, N.; Cushion, M.; Koziel, H. Pneumocystis-Mediated IL-8 Release by Macrophages Requires Coexpression of Mannose Receptors and TLR2. *Journal of Leukocyte Biology* **2007**, *81* (1), 205–211. https://doi.org/10.1189/jlb.1005580.

(5) Li, F.; Wang, H.; Li, Y.-Q.; Gu, Y.; Jia, X.-M. C-Type Lectin Receptor 2d Forms Homodimers and Heterodimers with TLR2 to Negatively Regulate IRF5-Mediated Antifungal Immunity. *Nat Commun* **2023**, *14* (1), 6718. https://doi.org/10.1038/s41467-023-42216-3.

(6) Geijtenbeek, T. B. H.; Gringhuis, S. I. Signalling through C-Type Lectin Receptors: Shaping Immune Responses. *Nat Rev Immunol* **2009**, *9* (7), 465–479. https://doi.org/10.1038/nri2569.

(7) den Dunnen, J.; Gringhuis, S. I.; Geijtenbeek, T. B. H. Innate Signaling by the C-Type Lectin DC-SIGN Dictates Immune Responses. *Cancer Immunol Immunother* **2009**, *58* (7), 1149–1157. https://doi.org/10.1007/s00262-008-0615-1.

(8) Park, D. D.; Chen, J.; Kudelka, M. R.; Jia, N.; Haller, C. A.; Kosaraju, R.; Premji, A. M.; Galizzi, M.; Nairn, A. V.; Moremen, K. W.; Cummings, R. D.; Chaikof, E. L. Resident and Elicited Murine Macrophages Differ in Expression of Their Glycomes and Glycan-Binding Proteins. *Cell Chemical Biology* **2021**, *28* (4), 567-582.e4. https://doi.org/10.1016/j.chembiol.2020.12.005.

(9) Cummings, R. D. The Mannose Receptor Ligands and the Macrophage Glycome. *Current Opinion in Structural Biology* **2022**, *75*, 102394. https://doi.org/10.1016/j.sbi.2022.102394.

(10) Tommasone, S.; Allabush, F.; Tagger, Y. K.; Norman, J.; Köpf, M.; Tucker, J. H. R.; Mendes, P. M. The Challenges of Glycan Recognition with Natural and Artificial Receptors. *Chem. Soc. Rev.* **2019**, *48* (22), 5488–5505. https://doi.org/10.1039/C8CS00768C.

(11) Riera, R.; Hogervorst, T. P.; Doelman, W.; Ni, Y.; Pujals, S.; Bolli, E.; Codée, J. D. C.; van Kasteren, S. I.; Albertazzi, L. Single-Molecule Imaging of Glycan–Lectin Interactions on Cells with Glyco-PAINT. *Nat Chem Biol* **2021**, *17* (12), 1281–1288. https://doi.org/10.1038/s41589-021-00896-2.

(12) Schnitzbauer, J.; Strauss, M. T.; Schlichthaerle, T.; Schueder, F.; Jungmann, R. Super-Resolution Microscopy with DNA-PAINT. *Nat Protoc* **2017**, *12* (6), 1198–1228. https://doi.org/10.1038/nprot.2017.024.

(13) van der Zande, H. J. P.; Nitsche, D.; Schlautmann, L.; Guigas, B.; Burgdorf, S. The Mannose Receptor: From Endocytic Receptor and Biomarker to Regulator of (Meta)Inflammation. *Front. Immunol.* **2021**, *12*, 765034. https://doi.org/10.3389/fimmu.2021.765034.

(14) Stahl, P. D.; Rodman, J. S.; Miller, M. J.; Schlesinger, P. H. Evidence for Receptor-Mediated Binding of Glycoproteins, Glycoconjugates, and Lysosomal Glycosidases by Alveolar Macrophages. *Proc. Natl. Acad. Sci. U.S.A.* **1978**, *75* (3), 1399–1403. https://doi.org/10.1073/pnas.75.3.1399.

(15) Stahl, P. D.; Ezekowitz, R. A. B. The Mannose Receptor Is a Pattern Recognition Receptor Involved in Host Defense. *Current opinion in immunology* **1998**, *10* (1), 50–55.

(16) Brown, G. D.; Willment, J. A.; Whitehead, L. C-Type Lectins in Immunity and Homeostasis. *Nat Rev Immunol* **2018**, *18* (6), 374–389. https://doi.org/10.1038/s41577-018-0004-8.

(17) Taylor, P. R.; Gordon, S.; Martinez-Pomares, L. The Mannose Receptor: Linking Homeostasis and Immunity through Sugar Recognition. *Trends in Immunology* **2005**, *26* (2), 104–110. https://doi.org/10.1016/j.it.2004.12.001.

(18) Feinberg, H.; Jégouzo, S. A. F.; Lasanajak, Y.; Smith, D. F.; Drickamer, K.; Weis, W. I.; Taylor, M. E. Structural Analysis of Carbohydrate Binding by the Macrophage Mannose Receptor CD206. *Journal of Biological Chemistry* **2021**, *296*. https://doi.org/10.1016/j.jbc.2021.100368.

(19) Solinas, G.; Schiarea, S.; Liguori, M.; Fabbri, M.; Pesce, S.; Zammataro, L.; Pasqualini, F.; Nebuloni, M.; Chiabrando, C.; Mantovani, A.; Allavena, P. Tumor-Conditioned Macrophages Secrete Migration-Stimulating Factor: A New Marker for M2-Polarization, Influencing Tumor Cell Motility. *The Journal of Immunology* **2010**, *185* (1), 642–652. https://doi.org/10.4049/jimmunol.1000413.

(20) Schuette, V.; Embgenbroich, M.; Ulas, T.; Welz, M.; Schulte-Schrepping, J.; Draffehn, A. M.; Quast, T.; Koch, K.; Nehring, M.; König, J.; Zweynert, A.; Harms, F. L.; Steiner, N.; Limmer, A.; Förster, I.; Berberich-Siebelt, F.; Knolle, P. A.; Wohlleber, D.; Kolanus, W.; Beyer, M.; Schultze, J. L.; Burgdorf, S. Mannose Receptor Induces T-Cell Tolerance via Inhibition of CD45 and up-Regulation of CTLA-4. *Proceedings of the National Academy of Sciences* **2016**, *113* (38), 10649–10654. https://doi.org/10.1073/pnas.1605885113.

(21) Mastrotto, F.; Pirazzini, M.; Negro, S.; Salama, A.; Martinez-Pomares, L.; Mantovani, G. Sulfation at Glycopolymer Side Chains Switches Activity at the Macrophage Mannose Receptor (CD206) In Vitro and In Vivo. *J. Am. Chem. Soc.* **2022**, *144* (50), 23134–23147. https://doi.org/10.1021/jacs.2c10757.

(22) Martinez-Pomares, L. The Mannose Receptor. *Journal of Leukocyte Biology* **2012**, *92* (6), 1177–1186. https://doi.org/10.1189/jlb.0512231.

(23) Napper, C. E.; Drickamer, K.; Taylor, M. E. Collagen Binding by the Mannose Receptor Mediated through the Fibronectin Type II Domain. *Biochemical Journal* **2006**, *395* (3), 579–586. https://doi.org/10.1042/BJ20052027.

(24) Mullin, N. P.; Hitchen, P. G.; Taylor, M. E. Mechanism of Ca2- and Monosaccharide Binding to a C-Type Carbohydrate-Recognition Domain of the Macrophage Mannose Receptor *. *Journal of Biological Chemistry* **1997**, *272* (9), 5668–5681. https://doi.org/10.1074/jbc.272.9.5668.

(25) Stavenhagen, K.; Mehta, A. Y.; Laan, L.; Gao, C.; Heimburg-Molinaro, J.; van Die, I.; Cummings, R. D. N-Glycosylation of Mannose Receptor (CD206) Regulates Glycan Binding by C-Type Lectin Domains. *J Biol Chem* **2022**, *298* (12), 102591. https://doi.org/10.1016/j.jbc.2022.102591.

(26) Schweizer, A.; Stahl, P. D.; Rohrer, J. A Di-Aromatic Motif in the Cytosolic Tail of the Mannose Receptor Mediates Endosomal Sorting. *J Biol Chem* **2000**, *275* (38), 29694–29700. https://doi.org/10.1074/jbc.M000571200.

(27) Rajaram, M. V. S.; Arnett, E.; Azad, A. K.; Guirado, E.; Ni, B.; Gerberick, A. D.; He, L.-Z.; Keler, T.; Thomas, L. J.; Lafuse, W. P.; Schlesinger, L. S. M. Tuberculosis-Initiated Human Mannose Receptor Signaling Temporally Regulates Macrophage Recognition and Vesicle Trafficking by FcRγ-Chain, Grb2 and SHP-1. *Cell Rep* **2017**, *21* (1), 126–140. https://doi.org/10.1016/j.celrep.2017.09.034.

(28) Kang, P. B.; Azad, A. K.; Torrelles, J. B.; Kaufman, T. M.; Beharka, A.; Tibesar, E.; DesJardin, L. E.; Schlesinger, L. S. The Human Macrophage Mannose Receptor Directs Mycobacterium Tuberculosis Lipoarabinomannan-Mediated Phagosome Biogenesis. *J Exp Med* **2005**, *202* (7), 987–999. https://doi.org/10.1084/jem.20051239.

(29) Burgdorf, S.; Kurts, C. Endocytosis Mechanisms and the Cell Biology of Antigen Presentation. *Current Opinion in Immunology* **2008**, *20* (1), 89–95. https://doi.org/10.1016/j.coi.2007.12.002.

(30) Hogervorst, T. P.; Li, R. J. E.; Marino, L.; Bruijns, S. C. M.; Meeuwenoord, N. J.; Filippov, D. V.; Overkleeft, H. S.; van der Marel, G. A.; van Vliet, S. J.; van Kooyk, Y.; Codée, J. D. C. *C* -Mannosyl Lysine for Solid Phase Assembly of Mannosylated Peptide Conjugate Cancer Vaccines. *ACS Chem. Biol.* **2020**, *15* (3), 728–739. https://doi.org/10.1021/acschembio.9b00987.

(31) Li, R.-J. E.; Hogervorst, T. P.; Achilli, S.; Bruijns, S. C.; Arnoldus, T.; Vivès, C.; Wong, C. C.; Thépaut, M.; Meeuwenoord, N. J.; van den Elst, H.; Overkleeft, H. S.; van der Marel, G. A.; Filippov, D. V.; van Vliet, S. J.; Fieschi, F.; Codée, J. D. C.; van Kooyk, Y. Systematic Dual Targeting of Dendritic Cell C-Type Lectin Receptor DC-SIGN and TLR7 Using a Trifunctional Mannosylated Antigen. *Front. Chem.* **2019**, *7*, 650. https://doi.org/10.3389/fchem.2019.00650.

(32) McIntosh, J. D.; Brimble, M. A.; Brooks, A. E. S.; Dunbar, P. R.; Kowalczyk, R.; Tomabechi, Y.; Fairbanks, A. J. Convergent Chemo-Enzymatic Synthesis of Mannosylated Glycopeptides; Targeting of Putative Vaccine Candidates to Antigen Presenting Cells. *Chem. Sci.* **2015**, *6* (8), 4636–4642. https://doi.org/10.1039/C5SC00952A.

(33) Segura, E.; Gupta, N.; Albiston, A. L.; Wicks, I. P.; Chai, S. Y.; Villadangos, J. A. Reply to Burgdorf et al.: The Mannose Receptor Is Not Involved in Antigen Cross-Presentation by Steady-State Dendritic Cells. *Proc. Natl. Acad. Sci. U.S.A.* **2010**, *107* (13). https://doi.org/10.1073/pnas.1001014107.

(34) Segura, E.; Albiston, A. L.; Wicks, I. P.; Chai, S. Y.; Villadangos, J. A. Different Cross-Presentation Pathways in Steady-State and Inflammatory Dendritic Cells. *Proceedings of the National Academy of Sciences* **2009**, *106* (48), 20377–20381.

(35) Burgdorf, S.; Schuette, V.; Semmling, V.; Hochheiser, K.; Lukacs-Kornek, V.; Knolle, P. A.; Kurts, C. Steady-State Cross-Presentation of OVA Is Mannose Receptor-Dependent but Inhibitable by Collagen Fragments. *Proc. Natl. Acad. Sci. U.S.A.* **2010**, *107* (13). https://doi.org/10.1073/pnas.1000598107.

(36) Burgdorf, S.; Kautz, A.; Böhnert, V.; Knolle, P. A.; Kurts, C. Distinct Pathways of Antigen Uptake and Intracellular Routing in CD4 and CD8 T Cell Activation. *Science* **2007**, *316* (5824), 612–616. https://doi.org/10.1126/science.1137971.

(37) Singh, S. K.; Streng-Ouwehand, I.; Litjens, M.; Kalay, H.; Burgdorf, S.; Saeland, E.; Kurts, C.; Unger, W. W.; van Kooyk, Y. Design of Neo-Glycoconjugates That Target the Mannose Receptor and Enhance TLR-Independent Cross-Presentation and Th1 Polarization. *European Journal of Immunology* **2011**, *41* (4), 916–925. https://doi.org/10.1002/eji.201040762.

(38) Rauen, J.; Kreer, C.; Paillard, A.; van Duikeren, S.; Benckhuijsen, W. E.; Camps, M. G.; Valentijn, A. R. P. M.; Ossendorp, F.; Drijfhout, J. W.; Arens, R.; Burgdorf, S. Enhanced Cross-Presentation and Improved CD8+ T Cell Responses after Mannosylation of Synthetic Long Peptides in Mice. *PLoS ONE* **2014**, *9* (8), e103755. https://doi.org/10.1371/journal.pone.0103755.

(39) Inaba, K.; Inaba, M.; Romani, N.; Aya, H.; Deguchi, M.; Ikehara, S.; Muramatsu, S.; Steinman, R. M. Generation of Large Numbers of Dendritic Cells from Mouse Bone Marrow Cultures Supplemented with Granulocyte/Macrophage Colony-Stimulating Factor. *J Exp Med* **1992**, *176* (6), 1693–1702. https://doi.org/10.1084/jem.176.6.1693.

(40) Gawden-Bone, C.; West, M. A.; Morrison, V. L.; Edgar, A. J.; McMillan, S. J.; Dill, B. D.; Trost, M.; Prescott, A.; Fagerholm, S. C.; Watts, C. A Crucial Role for B2 Integrins in Podosome Formation, Dynamics and Toll-like-Receptor-Signaled Disassembly in Dendritic Cells. *J Cell Sci* **2014**, *127* (Pt 19), 4213–4224. https://doi.org/10.1242/jcs.151167.

(41) van den Dries, K.; van Helden, S. F. G.; Riet, J. te; Diez-Ahedo, R.; Manzo, C.; Oud, M. M.; van Leeuwen, F. N.; Brock, R.; Garcia-Parajo, M. F.; Cambi, A.; Figdor, C. G. Geometry Sensing by Dendritic Cells Dictates Spatial Organization and PGE2-Induced Dissolution of Podosomes. *Cell Mol Life Sci* **2011**, *69* (11), 1889–1901. https://doi.org/10.1007/s00018-011-0908-y.

(42) *TrackMate 7: integrating state-of-the-art segmentation algorithms into tracking pipelines | Nature Methods*. https://www.nature.com/articles/s41592-022-01507-1 (accessed 2024-07-26).

(43) R Core Team. *R: A Language and Environment for Statistical Computing*; R Foundation for Statistical Computing: Vienna, Austria, 2023.

(44) Hogquist, K. A.; Jameson, S. C.; Heath, W. R.; Howard, J. L.; Bevan, M. J.; Carbone, F. R. T Cell Receptor Antagonist Peptides Induce Positive Selection. *Cell* **1994**, *76* (1), 17–27. https://doi.org/10.1016/0092-8674(94)90169-4.

(45) Streng-Ouwehand, I.; Ho, N. I.; Litjens, M.; Kalay, H.; Boks, M. A.; Cornelissen, L. A.; Kaur Singh, S.; Saeland, E.; Garcia-Vallejo, J. J.; Ossendorp, F. A.; Unger, W. W.; van Kooyk, Y. Glycan Modification of Antigen Alters Its Intracellular Routing in Dendritic Cells, Promoting Priming of T Cells. *eLife* **2016**, *5*, e11765. https://doi.org/10.7554/eLife.11765.

(46) Rostovtsev, V. V.; Green, L. G.; Fokin, V. V.; Sharpless, K. B. A Stepwise Huisgen Cycloaddition Process: Copper(I)-Catalyzed Regioselective "Ligation" of Azides and Terminal Alkynes. *Angewandte Chemie International Edition* **2002**, *41* (14), 2596–2599. https://doi.org/10.1002/1521-3773(20020715)41:14<2596::AID-ANIE2596>3.0.CO;2-4.

(47) Tornøe, C. W.; Christensen, C.; Meldal, M. Peptidotriazoles on Solid Phase: [1,2,3]-Triazoles by Regiospecific Copper(I)-Catalyzed 1,3-Dipolar Cycloadditions of Terminal Alkynes to Azides. *J. Org. Chem.* **2002**, *67* (9), 3057–3064. https://doi.org/10.1021/jo011148j.

(48) Le Guével, X.; Perez Perrino, M.; Fernández, T. D.; Palomares, F.; Torres, M.-J.; Blanca, M.; Rojo, J.; Mayorga, C. Multivalent Glycosylation of Fluorescent Gold Nanoclusters

Promotes Increased Human Dendritic Cell Targeting via Multiple Endocytic Pathways. *ACS Appl. Mater. Interfaces* **2015**, *7* (37), 20945–20956. https://doi.org/10.1021/acsami.5b06541.

(49) Khalil, I. A.; Kogure, K.; Akita, H.; Harashima, H. Uptake Pathways and Subsequent Intracellular Trafficking in Nonviral Gene Delivery. *Pharmacol Rev* **2006**, *58* (1), 32–45. https://doi.org/10.1124/pr.58.1.8.

(50) Park, Y.; Abihssira-García, I. S.; Thalmann, S.; Wiegertjes, G. F.; Barreda, D. R.; Olsvik, P. A.; Kiron, V. Imaging Flow Cytometry Protocols for Examining Phagocytosis of Microplastics and Bioparticles by Immune Cells of Aquatic Animals. *Front. Immunol.* **2020**, *11*. https://doi.org/10.3389/fimmu.2020.00203.

(51) Kimura, T.; Nada, S.; Takegahara, N.; Okuno, T.; Nojima, S.; Kang, S.; Ito, D.; Morimoto, K.; Hosokawa, T.; Hayama, Y.; Mitsui, Y.; Sakurai, N.; Sarashina-Kida, H.; Nishide, M.; Maeda, Y.; Takamatsu, H.; Okuzaki, D.; Yamada, M.; Okada, M.; Kumanogoh, A. Polarization of M2 Macrophages Requires Lamtor1 That Integrates Cytokine and Amino-Acid Signals. *Nat Commun* **2016**, *7* (1), 13130. https://doi.org/10.1038/ncomms13130.

(52) Rillahan, C. D.; Paulson, J. C. Glycan Microarrays for Decoding the Glycome. *Annu. Rev. Biochem.* **2011**, *80* (1), 797–823. https://doi.org/10.1146/annurev-biochem-061809-152236.

(53) Shinohara, Y.; Furukawa, J. Surface Plasmon Resonance as a Tool to Characterize Lectin-Carbohydrate Interactions. *Methods Mol Biol* **2014**, *1200*, 185–205. https://doi.org/10.1007/978-1-4939-1292-6_17.

(54) Kéry, V.; Krepinský, J. J.; Warren, C. D.; Capek, P.; Stahl, P. D. Ligand Recognition by Purified Human Mannose Receptor. *Arch Biochem Biophys* **1992**, *298* (1), 49–55. https://doi.org/10.1016/0003-9861(92)90092-b.

(55) E. Tholen, M. M.; P. Tas, R.; Wang, Y.; Albertazzi, L. Beyond DNA: New Probes for PAINT Super-Resolution Microscopy. *Chemical Communications* **2023**, *59* (54), 8332–8342. https://doi.org/10.1039/D3CC00757J.

(56) Tas, R. P.; Albertazzi, L.; Voets, I. K. Small Peptide–Protein Interaction Pair for Genetically Encoded, Fixation Compatible Peptide-PAINT. *Nano Lett.* **2021**, *21* (22), 9509–9516. https://doi.org/10.1021/acs.nanolett.1c02895.

(57) Albertazzi, L.; Heilemann, M. When Weak Is Strong: A Plea for Low-Affinity Binders for Optical Microscopy. *Angewandte Chemie International Edition* **2023**, *62* (35), e202303390. https://doi.org/10.1002/anie.202303390.

(58) Dustin, M. L. Recent Advances in Understanding TCR Signaling: A Synaptic Perspective. *Fac Rev* **2023**, *12*. https://doi.org/10.12703/r/12-25.

(59) *Mapping the stochastic sequence of individual ligand-receptor binding events to cellular activation: T cells act on the rare events | Science Signaling*. https://www.science.org/doi/full/10.1126/scisignal.aat8715 (accessed 2024-07-24).

(60) Yu, X.; Orr, C. M.; Chan, H. T. C.; James, S.; Penfold, C. A.; Kim, J.; Inzhelevskaya, T.; Mockridge, C. I.; Cox, K. L.; Essex, J. W.; Tews, I.; Glennie, M. J.; Cragg, M. S. Reducing Affinity as a Strategy to Boost Immunomodulatory Antibody Agonism. *Nature* **2023**, *614* (7948), 539–547. https://doi.org/10.1038/s41586-022-05673-2.

(61) Canton, J. Macropinocytosis: New Insights Into Its Underappreciated Role in Innate Immune Cell Surveillance. *Front. Immunol.* **2018**, *9*. https://doi.org/10.3389/fimmu.2018.02286.
(62) Liu, Z.; Roche, P. A. Macropinocytosis in Phagocytes: Regulation of MHC Class-II-Restricted Antigen Presentation in Dendritic Cells. *Front Physiol* **2015**, *6*, 1. https://doi.org/10.3389/fphys.2015.00001.
(63) Norbury, C. C.; Hewlett, L. J.; Prescott, A. R.; Shastri, N.; Watts, C. Class I MHC Presentation of Exogenous Soluble Antigen via Macropinocytosis in Bone Marrow Macrophages. *Immunity* **1995**, *3* (6), 783–791. https://doi.org/10.1016/1074-7613(95)90067-5.
(64) Watts, C.; West, M. A.; Zaru, R. TLR Signalling Regulated Antigen Presentation in Dendritic Cells. *Current Opinion in Immunology* **2010**, *22* (1), 124–130. https://doi.org/10.1016/j.coi.2009.12.005.
(65) Chatterjee, B.; Smed-Sörensen, A.; Cohn, L.; Chalouni, C.; Vandlen, R.; Lee, B.-C.; Widger, J.; Keler, T.; Delamarre, L.; Mellman, I. Internalization and Endosomal Degradation of Receptor-Bound Antigens Regulate the Efficiency of Cross Presentation by Human Dendritic Cells. *Blood* **2012**, *120* (10), 2011–2020. https://doi.org/10.1182/blood-2012-01-402370.

MAIN FIGURES

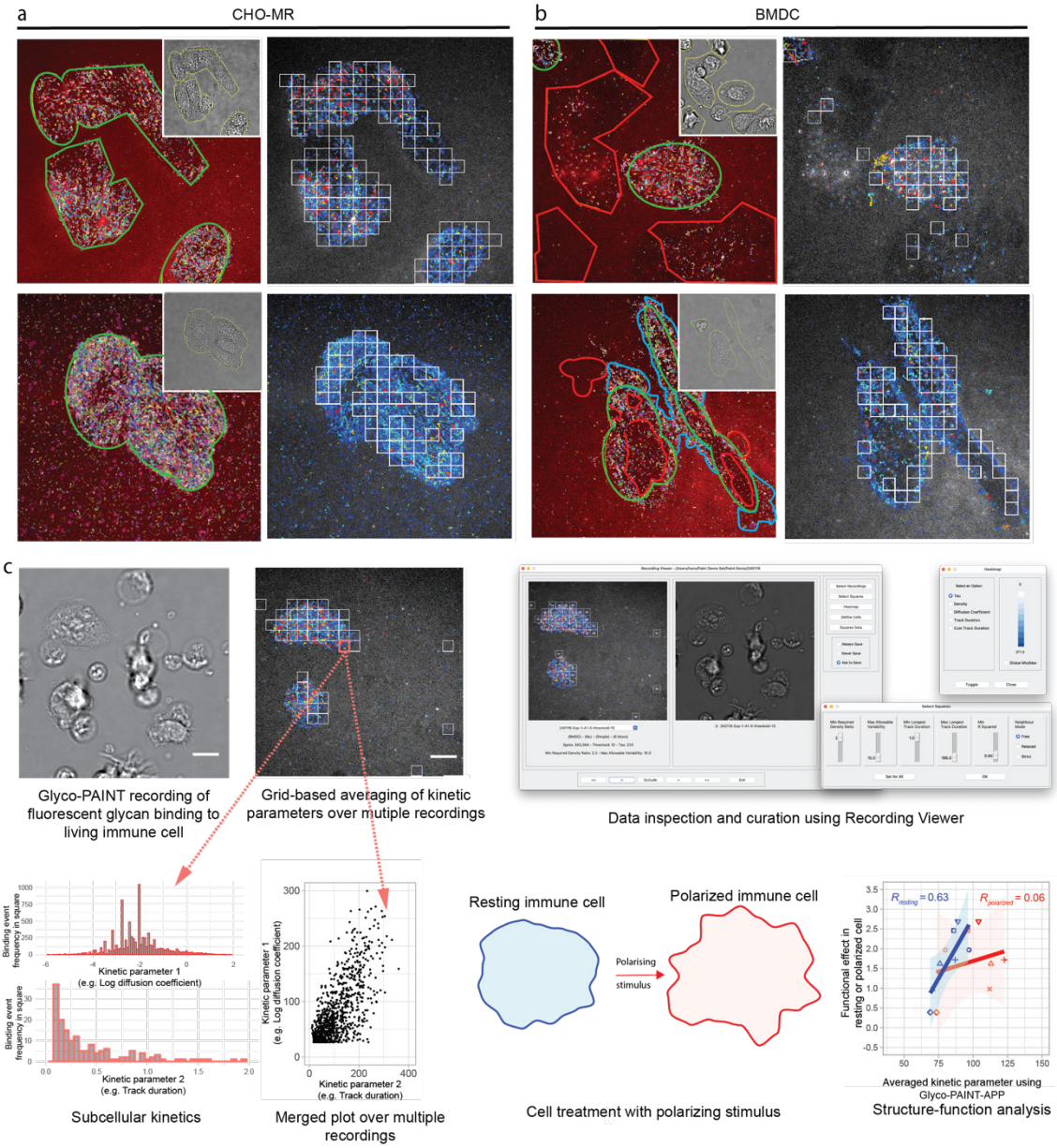

Figure 1 | Glyco-PAINT-APP allows subcellular analysis of immune cell lectin binding. A) Left images: original Glyco-PAINT analysis of fluorescent mannose glycan binding to CHO-MR cells. ROIs are drawn using brightfield-defined cell contours (inset, yellow outlines) and areas where binding events are overlapping with cell areas are outlined in green. Binding trajectories are randomly coloured. Right: Grid-based identification of binding events using Glyco-PAINT-APP. White-outlined squares show an independent selection of cell-related binding events and define the area over which events are integrated. **B)** Same as **A** but for BMDC. In the left images, non-overlapping areas devoid of binding events arising from primary cell intrinsic heterogeneity are outlined in red and areas engaging in binding events but outside of brightfield-defined cell outlines are coloured in blue. **C)** Overview of the Glyco-PAINT-APP workflow: primary

immune cells are cultured in a live-cell imaging chamber and a brightfield image is recorded. After addition of a fluorescent probe, spots are recorded using PAINT imaging and reconstructed into tracks reflecting glycan binding events which are then subdivided into squares of variable size depicting subcellular regions of live immune cells. Kinetic parameters such as on-, off-rates and diffusion coefficients of glycan ligands averaged per individual square can then be analyzed and filtered using the *Recording Viewer* tool and displayed as heatmaps, histograms or scatterplots. Kinetic parameters derived using the algorithm can then be correlated to functional effects of resting or polarized immune cells. Scalebars represent 10 µm, data figures indicate representative illustrative data

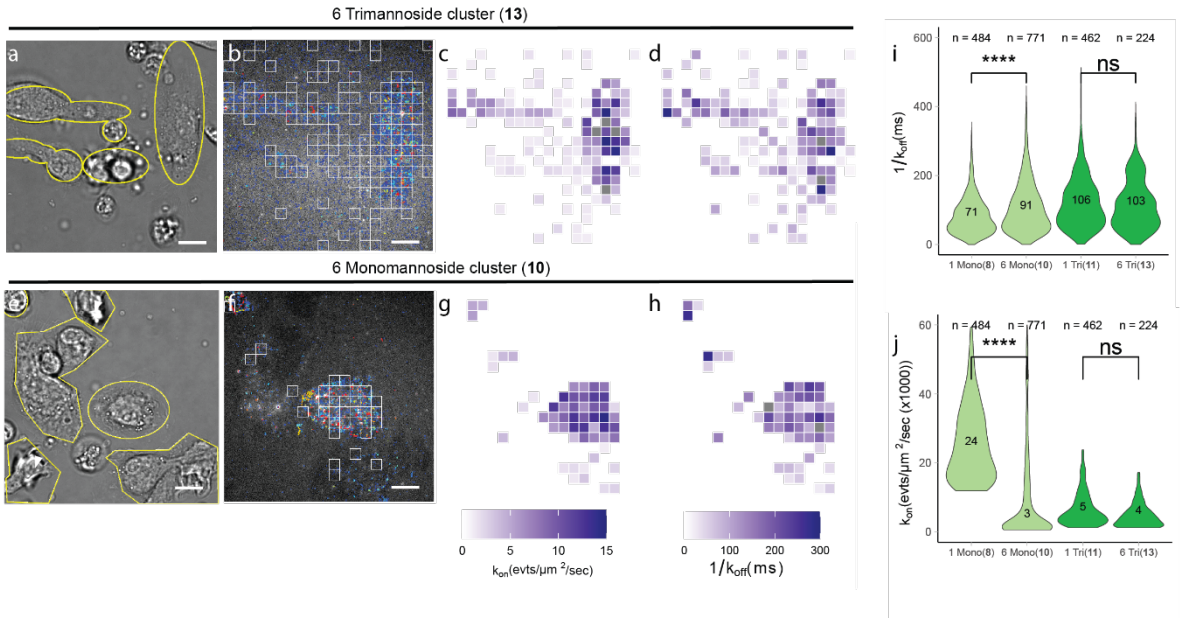

Figure 2 | Subcellular analysis of glycan binding on dendritic cells resolves averaging artefacts. A) brightfield image of live BMDCs. **B)** Reconstruction of binding events recorded with 5 nM trimannoside glycan **13** processed using a 20x20 grid with all squares that have passed selection criteria (*Density_Ratio* > 2, *R_Squared* > 0.9, *Nr_Tracks/square* > 20) displayed by white outlines (**Figure S3A, B** show the same set of images for glycan clusters **11** and **13**). **C)** Heatmap projection of the number of binding events/square showing the high heterogeneity of binding events even between the selected squares on the same cell. **D)** Heatmap display of τ per square. **E-H)** The same as **A-D** but for glycan cluster **10**. **I-J)** Violin distribution plots and median value of k_{on} and k_{off}^{-1} for all glycans **10-13**. n = the number of squares that were analyzed per violin. Significance was assessed using two-way ANOVA followed by a Tukey post-hoc test. Scalebars represent 10 µm. Tracks in **B** and **F** are colored from short to long track length (light blue to red).

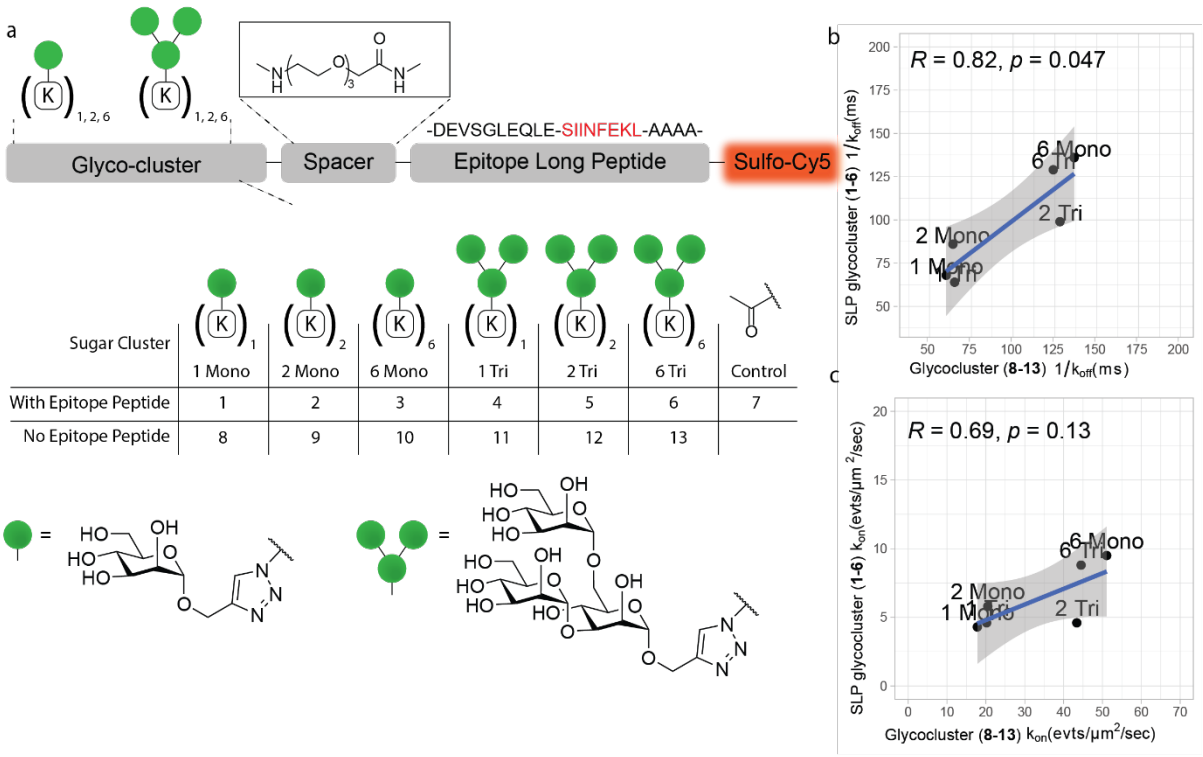

Figure 3 | Library of fluorescently labeled mannose ligands with SLP antigenic peptide. A) Design of synthetic glycoclusters. **1-7** carry an N-terminal long peptide from Ovalbumin$_{263\text{-}275}$ and a sulfo-Cy5 fluorophore on a C-terminal lysine side chain. Glycocluster series **8-13** do not contain this SLP, but are directly attached to an ATTO655 fluorophore. **B-C)** Correlation analysis of the median rel. k_{on} and k_{off}^{-1} between probes with identical glycan but bearing long peptide antigens binding to CHO-MR cells. Data points are medians for all squares analyzed with a 20x20 grid and filtered with *Density_Ratio* > 2, *R_Squared* > 0.9 and *Nr_Tracks/Square* > 20. Pearson's R and two-tailed t test P value are displayed in the correlation plots.

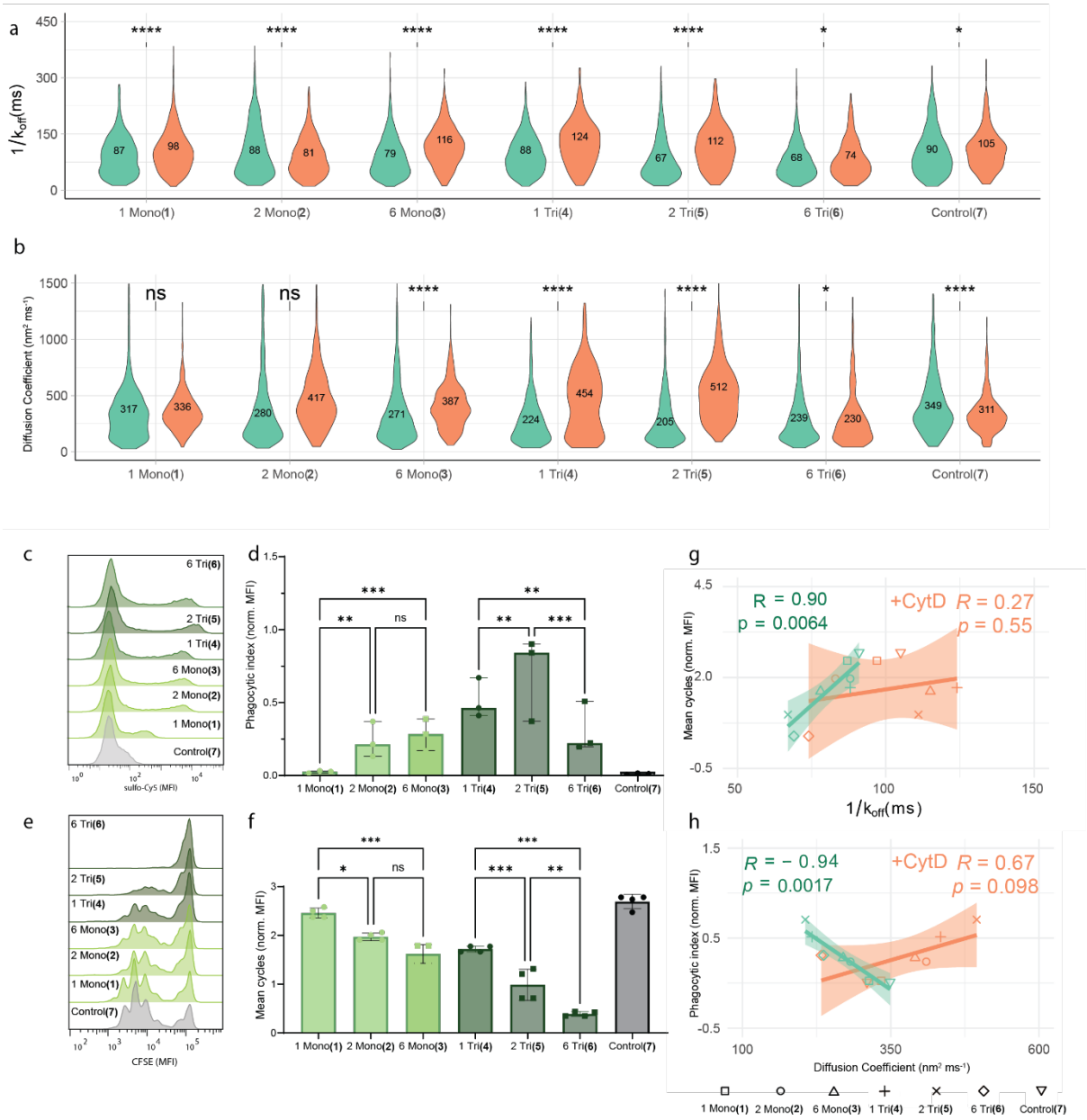

Figure 4 | Kinetic parameters correlate with ligand functionality. A) Distribution of k_{off}^{-1} for binding events between probes **1-7** and live untreated (green violins) or Cytochalasin D treated (red violins) BMDCs. Numerical median values are displayed in the violins. **B)** Same as in **A)** for the average diffusion coefficient per square. **C)** Histograms of BMDCs incubated with probe **1-7** for 1h and subsequent measurement of endocytosis in $CD11c^{+}$ cells using flow cytometry. **D)** Bar chart of **C)** as the phagocytic index. **E)** Histograms of CFSE dilution in dividing OT-I T cells that were cocultured for 3 days with mature BMDC that were pulsed for 2h with antigens **1-7** and measured using flow cytometry. **F)** Bar chart of the average number of cell divisions per T cell obtained from **E)**. **G)** Correlation between median k_{off}^{-1} for untreated or CytD treated cells and the mean number of T-cell divisions. **H)** Correlation between probe median diffusion coefficients for untreated or CytD treated cells and phagocytic index. Glyco-PAINT-APP analysis was done using a 20x20 grid and filtered with *Density_Ratio* > 2, *R_Squared* > 0.9 and *Nr_Tracks* > 20. Significance was

assessed using two-way ANOVA followed by a Tukey post-hoc test. Pearson's R and two-tailed t test P value are displayed in the correlation plots.

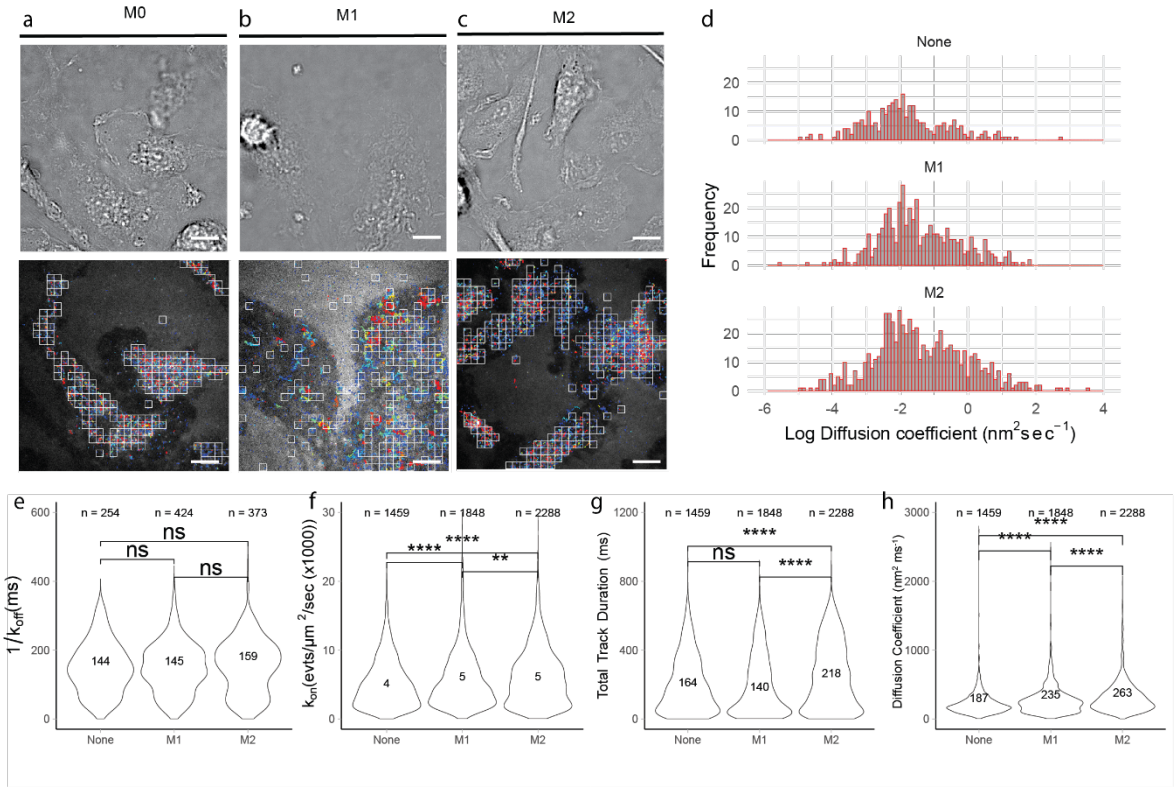

Figure 5 | Macrophage polarization alters glycan binding profile. A-C) Top: brightfield image live BMDM. Bottom: reconstruction of binding trajectories of glycan **13** to BMDM treated for 16h with no stimulus, an M1-inducing stimulus, or an M2-inducing stimulus. Recordings were processed using a grid sized 20x20 and squares with *Density_Ratio* > 10 and *Nr_Tracks* > 20 are displayed using white borders in the image. **D)** Distribution of diffusion coefficients obtained from the single square with highest event density per recording for the M0-M2 macrophage phenotypes showing the appearance of longer and faster moving tracks upon M2-polarisation. **E-H)** Violin distribution and median value of k_{off}^{-1}, k_{on}, total track durations and diffusion coefficients for glycan **13** binding to BMDM treated with different stimuli showing the appearance of longer binding tracks upon M2-polarization without a change in off rate. n = the number of squares from which the data were obtained. For **E** squares were additionally filtered using *R_Squared* > *0.8*. Significance was assessed using two-way ANOVA followed by a Tukey post-hoc test. Tracks are in colored from short to long track length (light blue to red).

Quantification of single molecule glycan-mannose receptor binding kinetics on myeloid cells reveals high subcellular binding heterogeneity

Kas Steuten[1], Johannes J.A. Bakker[1], Ward Doelman[1], Diana Torres-García[1], Roger Riera[2], Lorenzo Albertazzi[2], Sander I. van Kasteren[1]*

Department of Chemical Biology and Immunology, Leiden Institute of Chemistry, Leiden University, Leiden, the Netherlands[1]

Department of Biomedical Engineering and Institute for Complex Molecular Systems, Eindhoven University of Technology, Eindhoven, the Netherlands[2]

*Correspondence: s.i.van.kasteren@chem.leidenuniv.nl

Supplementary Information

SUPPLEMENTARY FIGURES 26

RESOURCE AVAILABILITY 35

EXPERIMENTAL MODEL DETAILS 35

EXPERIMENTAL METHOD DETAILS 36

REFERENCES 43

LC-MS ANALYSIS 44

SUPPLEMENTARY FIGURES

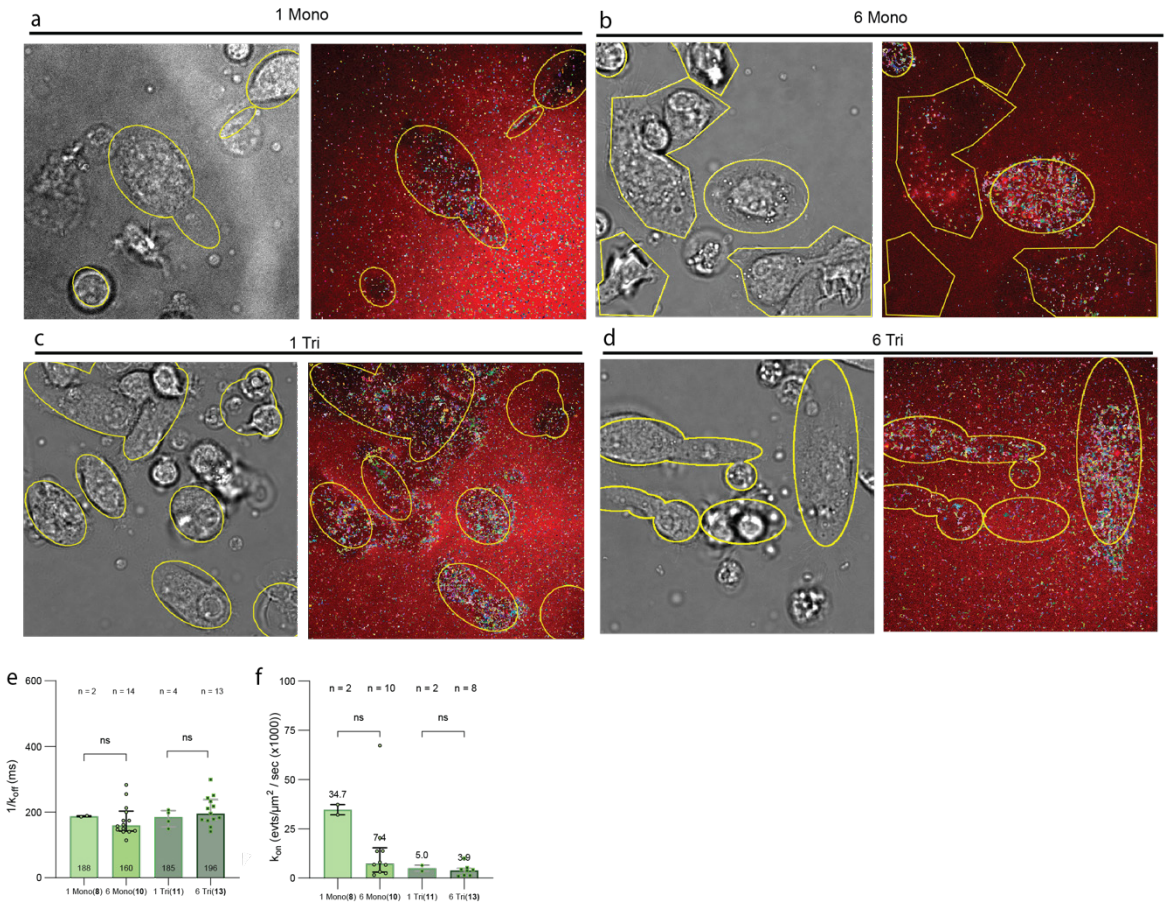

Figure S1 | Manual analysis of glycan binding on dendritic cells is complicated by intrinsic cell heterogeneity and results in averaging artefacts. A) BMDC were incubated with 5 nM of fluorescent mannoside **8** in a live cell imaging chamber and a brightfield image was captured followed by a 2000 frame Glyco-PAINT recording. Closely linked spots were reconstructed into tracks representing binding events using ImageJ TrackMate plugin and background filtering was performed by manual cell definition using ROI drawing (yellow areas). **B-D)** identical analysis for glycans **10**, **11** and **13,** respectively. **E)** Quantification of the number of events per area which is a relative measure of k_{on}. **F)** The average k_{off}^{-1} or τ for these events determined by fitting a one-phase exponential decay function over the binding event duration distribution histograms. n, depicts the number of FOVs that were analyzed in total and were acquired over at least 3 biological replicates. Significance was assessed using two-way ANOVA followed by a Tukey post-hoc test. Tracks are colored randomly.

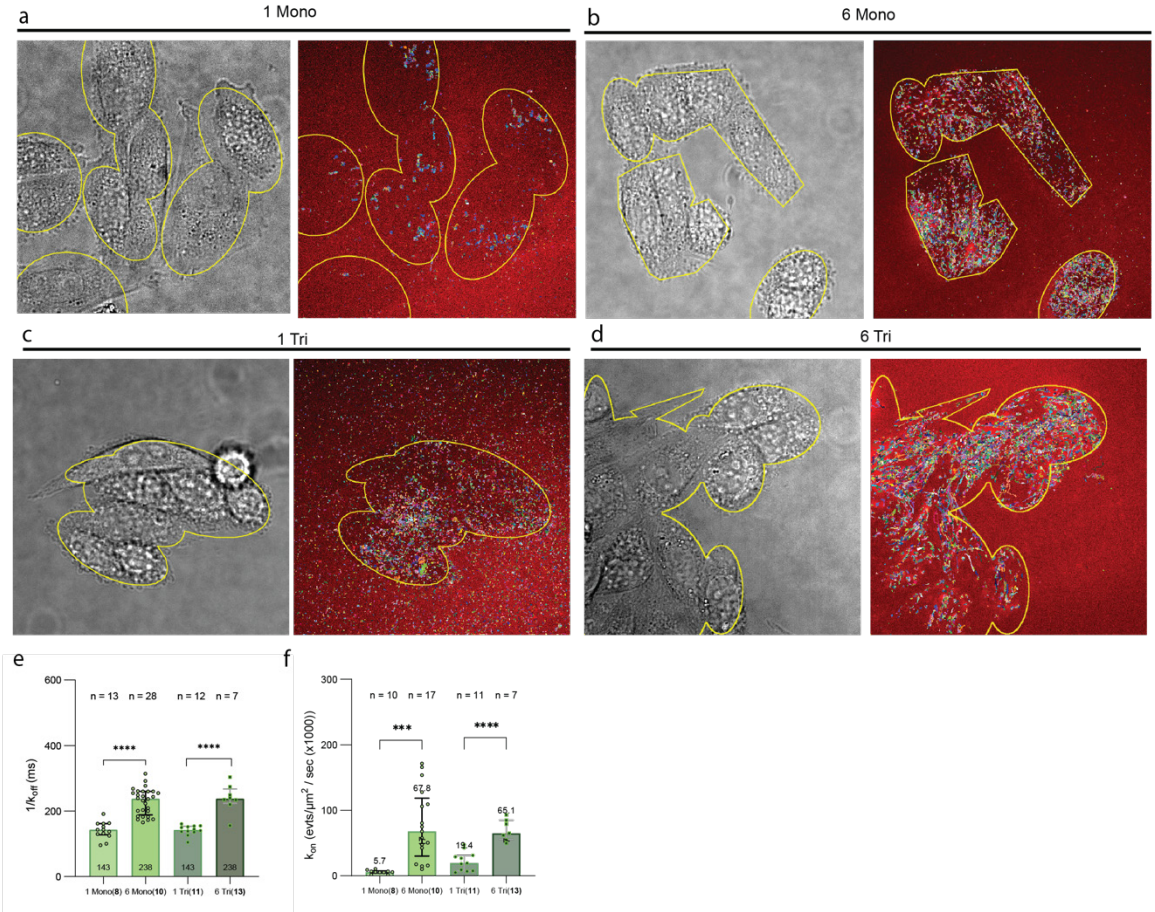

Figure S2 | Manual analysis of glycan binding to CHO-MR using original Glyco-PAINT method. A) CHO-MR cells were incubated with 1 nM of fluorescent mannoside **8** in a live cell imaging chamber and a brightfield image was captured followed by a 2000 frame Glyco-PAINT recording. Closely linked spots were reconstructed into tracks representing binding events using ImageJ TrackMate plugin and background filtering was performed by manual cell definition using ROI drawing (yellow areas). **B-D)** identical analysis for glycans **10**, **11** and **13,** respectively. **E)** Displays the number of events per area which is a relative measure of k_{on}. **F)** Displays the average k_{off}^{-1} for these events determined by fitting a one-phase exponential decay function over the binding event duration distribution histograms. n, depicts the number of FOVs that were analyzed in total and were acquired over at least 3 biological replicates. Significance was assessed using two-way ANOVA followed by a Tukey post-hoc test. Tracks are colored randomly.

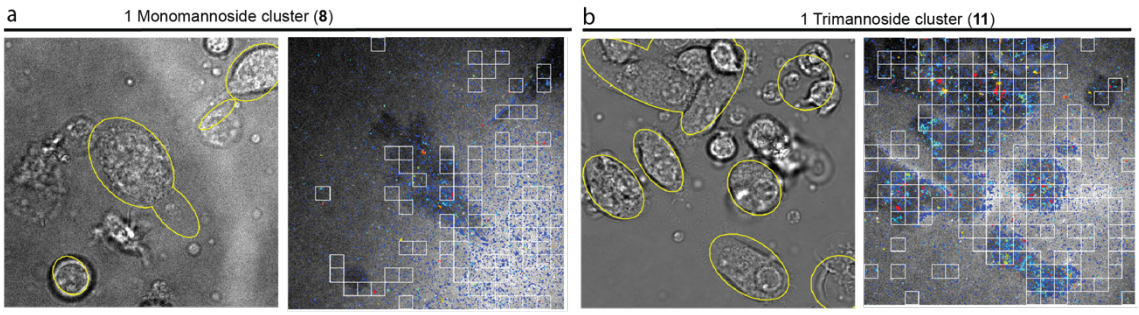

Figure S3 | Glyco-PAINT-APP analysis of glycan binding to dendritic cells. A-B) Additional to main **Figure 2.** Brightfield and square-based detection of binding events for representative recordings of glycans **8** and **11**. Analysis and selection parameters are identical as in **Figure 2**.

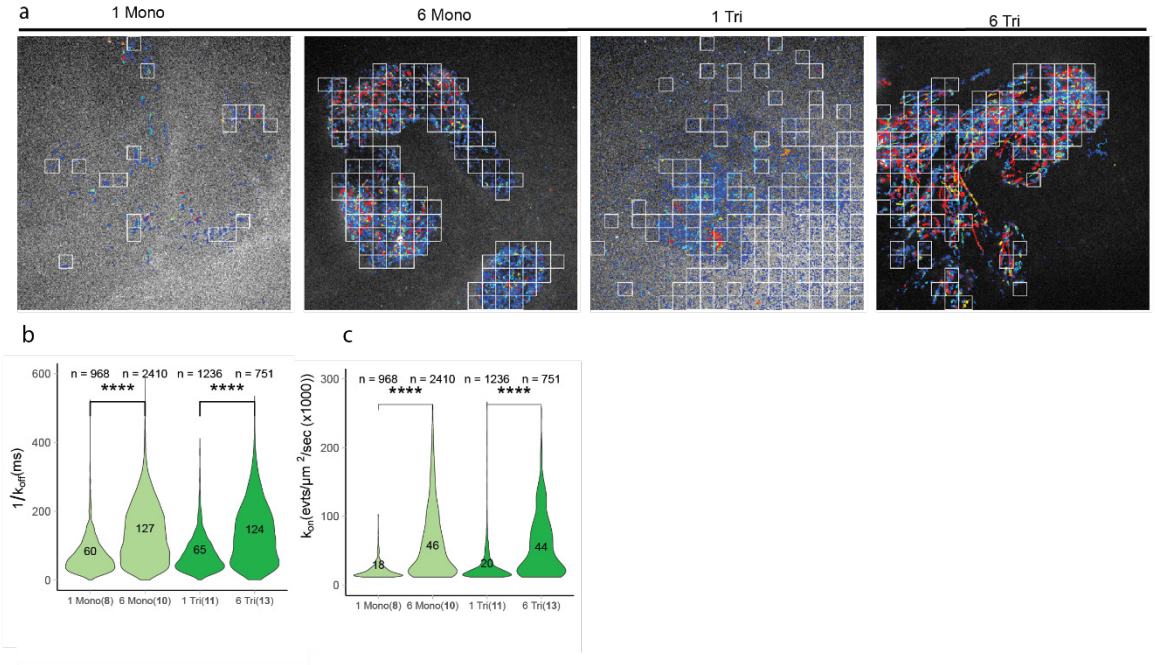

Figure S4 | Glyco-PAINT-APP analysis of glycan binding to CHO-MR. A) In addition to **Figure S2.** Square-based detection of binding events for representative recordings of glycans **8** and **11. A)** Square-based detection of **8, 10, 11** and **13** binding to CHO-MR, identical images as in shown in **Figure S2** using ROI analysis. **B)** The number of events per area which is a relative measure of k_{on}. **C)** average k_{off}^{-1} or τ for these events determined by fitting a one-phase exponential decay function over the binding event duration distribution histograms. n, depicts the number of FOVs that were analyzed in total and were acquired over at least 3 biological replicates. Recordings were analyzed using a 20x20 grid and filtered with *Density_Ratio* > 2, *R_Squared* > 0.9 and *Nr_Tracks* > 20. Significance was assessed using two-way ANOVA followed by a Tukey post-hoc test.

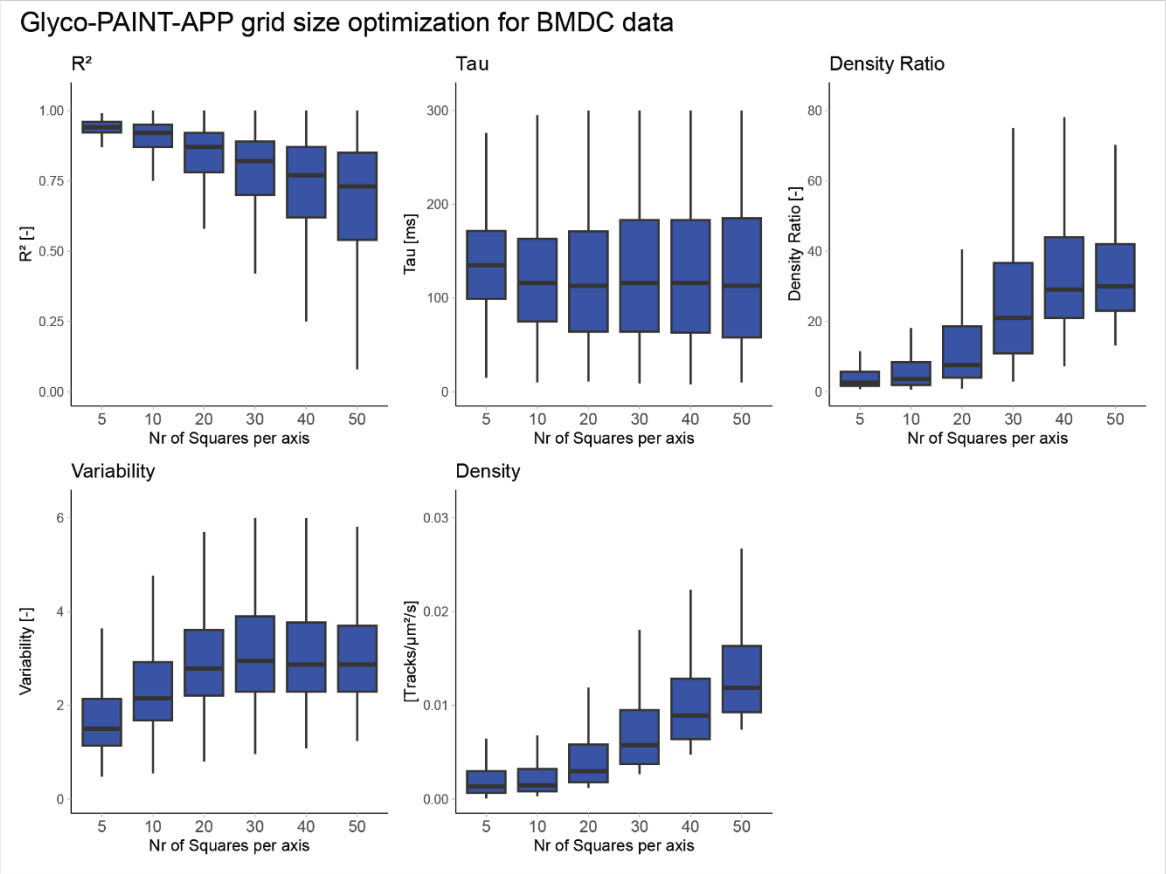

Figure S5 | Glyco-PAINT-APP grid size optimization for dendritic cells. Analysis of the effect of mesh size on kinetic and statistical parameters for glycan binding to DC.

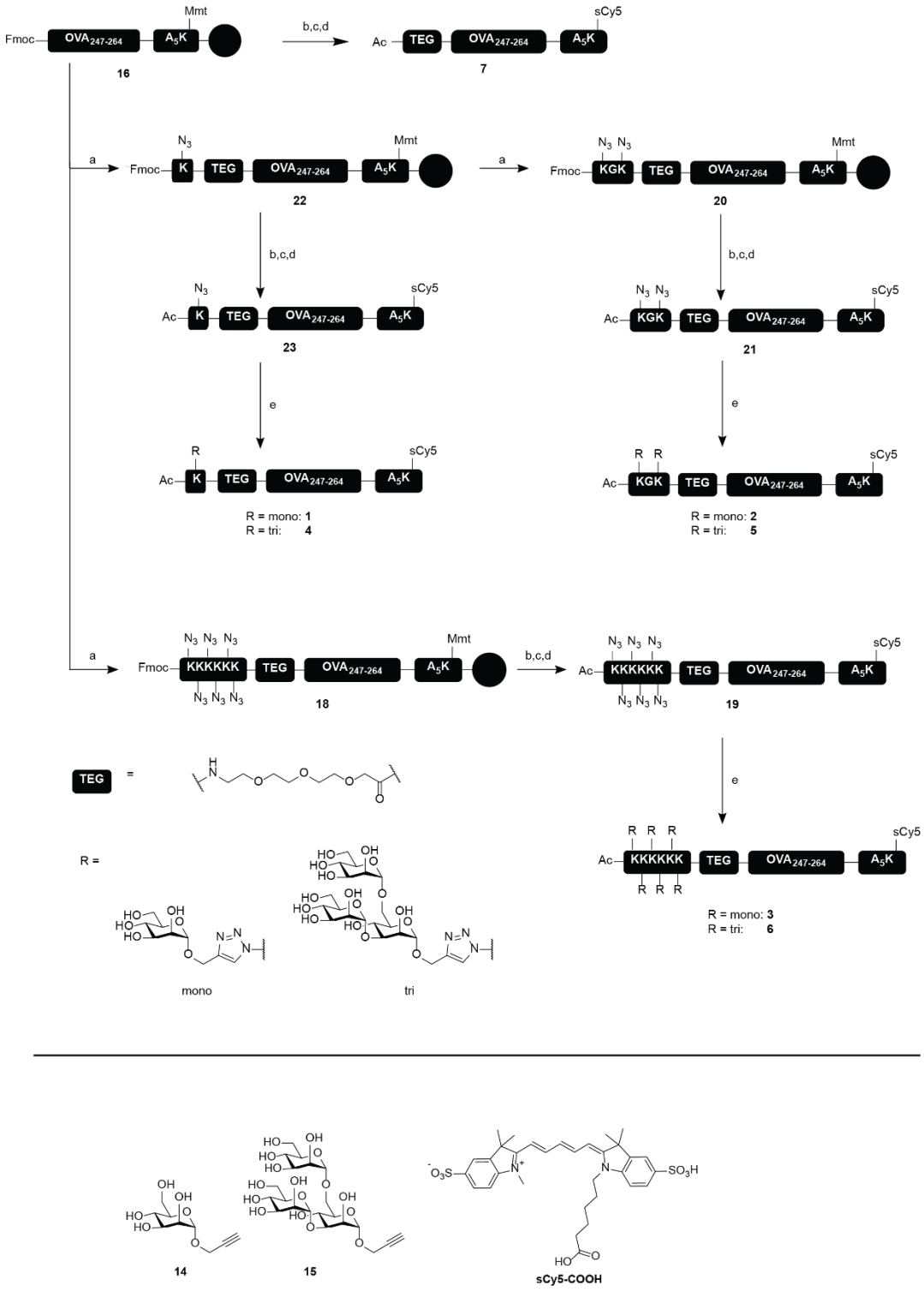

Figure S6 | **Synthetic scheme for glycopeptides 1-7.** Reagents and conditions: a) SPPS (HCTU, Fmoc-TEG-OH, Fmoc-Lys(N_3)-OH) b) i) 20 % (v/v) piperidine/DMF ii) Ac_2O, DiPEA, DMF c) i) AcOH, TFE, DCM ii) Et_3N, DMF iii) **sCy5-COOH**, HCTU, DiPEA, DMF d) i) TFA, TIS, H_2O ii) RP-HPLC e) i) **14** or **15**, $CuSO_4$,

809 NaAsc, THPTA, DMSO, 40°C ii) SEC. Synthetic procedures have been described for propargyl
810 mannosides **14** and **15** by Riera et al.[1] and Hogervorst and Li et al.[2] respectively.

811 **Table S1 | Median values of Glyco-PAINT-APP derived kinetics for probe 1-7 binding to BMDC and**
812 **CHO-MR.** Square selection criteria as in **Figure 4A-B**. Cells were treated with 10 µM Cytochalasin D for
813 30 min in indicated tables. TTD, total track duration LTD, long track duration. STD, short track duration.
814 DC, diffusion coefficient.

Cell Type	Adjuvant	Probe	Tau	Density	TTD	Avg LTD	Avg STD	DC	Avg Speed	Max Speed
CHOMR	None	1 Mono	68	4.2	16.2	1.52	0.1	200	2.1	3.2
CHOMR	None	2 Mono	91	6.3	25.8	1.50	0.1	354	2.3	4.5
CHOMR	None	6 Mono	117	10.3	46.2	1.40	0.1	371	2.1	4.5
CHOMR	None	1 Tri	79	4.9	17.9	1.52	0.1	211	1.7	3.2
CHOMR	None	2 Tri	117	3.6	14.5	1.38	0.1	333	1.9	3.2
CHOMR	None	6 Tri	101	6.8	29.0	1.75	0.1	354	2.3	4.5
CHOMR	None	Control	74	7.6	26.9	1.30	0.1	159	1.6	3.2
CHOMR	CytD	1 Mono	63	3.8	9.8	0.95	0.1	98	1.6	3.2
CHOMR	CytD	2 Mono	85	5.7	15.5	1.02	0.1	241	2.2	4.5
CHOMR	CytD	6 Mono	115	10.7	32.8	1.14	0.1	525	2.6	4.5
CHOMR	CytD	1 Tri	144	15.3	52.4	1.30	0.1	448	2.6	4.5
CHOMR	CytD	2 Tri	108	7.2	31.9	1.40	0.1	384	2.3	4.5
CHOMR	CytD	6 Tri	85	5.2	12.6	0.90	0.1	296	2.4	4.5
CHOMR	CytD	Control	55	3.7	9.9	1.12	0.1	188	2.3	3.9
BMDC	None	1 Mono	87	1.8	10.9	1.12	0.1	317	2.2	4.5
BMDC	None	2 Mono	96	2.2	16.5	1.70	0.1	317	2.6	4.5
BMDC	None	6 Mono	76	2.3	19.9	1.62	0.1	266	2.1	4.5
BMDC	None	1 Tri	88	1.6	13.6	1.25	0.1	224	1.6	3.2
BMDC	None	2 Tri	69	1.5	12.1	1.65	0.1	211	1.9	3.2
BMDC	None	6 Tri	68	2.1	15.8	1.55	0.1	239	2.1	4.5
BMDC	None	Control	90	2.0	13.7	1.15	0.1	349	2.4	4.5
BMDC	CytD	1 Mono	98	2.3	11.8	1.00	0.1	336	2.1	3.3
BMDC	CytD	2 Mono	81	2.4	15.4	1.23	0.1	417	2.7	4.5
BMDC	CytD	6 Mono	116	1.6	9.6	1.00	0.1	387	2.4	4.5
BMDC	CytD	1 Tri	124	2.2	16.4	1.12	0.1	454	2.3	4.5
BMDC	CytD	2 Tri	112	1.7	12.4	1.10	0.1	512	2.7	4.5
BMDC	CytD	6 Tri	74	2.0	12.8	1.23	0.1	230	2.1	4.5
BMDC	CytD	Control	105	2.0	12.0	1.05	0.1	311	2.1	3.8

815

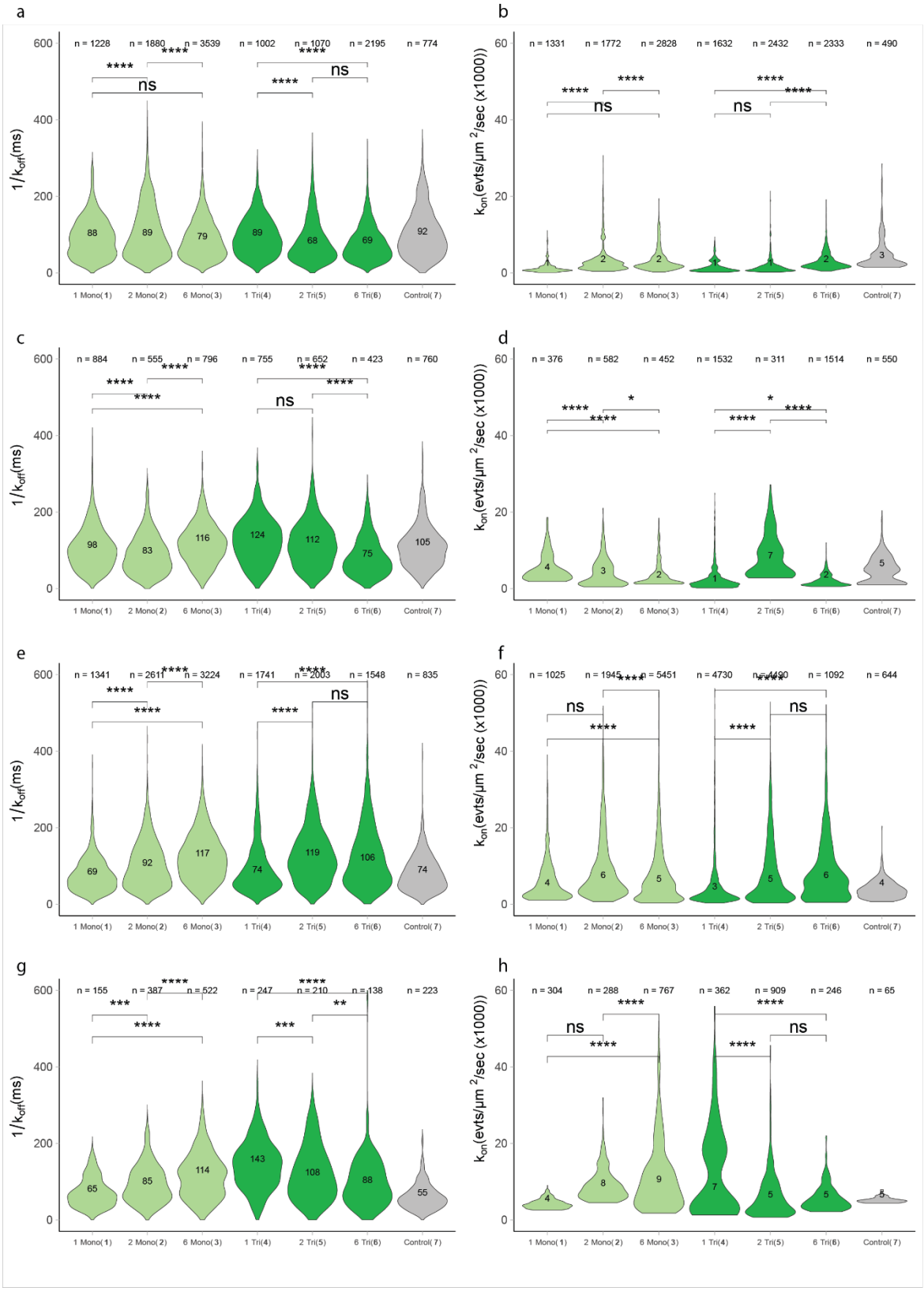

816
817 **Figure S7 | Violin distribution of Glyco-PAINT-APP derived k_{on} and k_{off}^{-1} for probe 1-7 binding to BMDC**
818 **and CHO-MR.** Square selection criteria as in main **Figure 4. A,B** BMDC, **C,D** BMDC treated with
819 cytochalasin D, **E,F** CHO-MR and **G,H** CHO-MR treated with cytochalasin D. n, indicates the number of

820 squares that were selected. Significance was assessed using two-way ANOVA followed by a Tukey post-
821 hoc test.

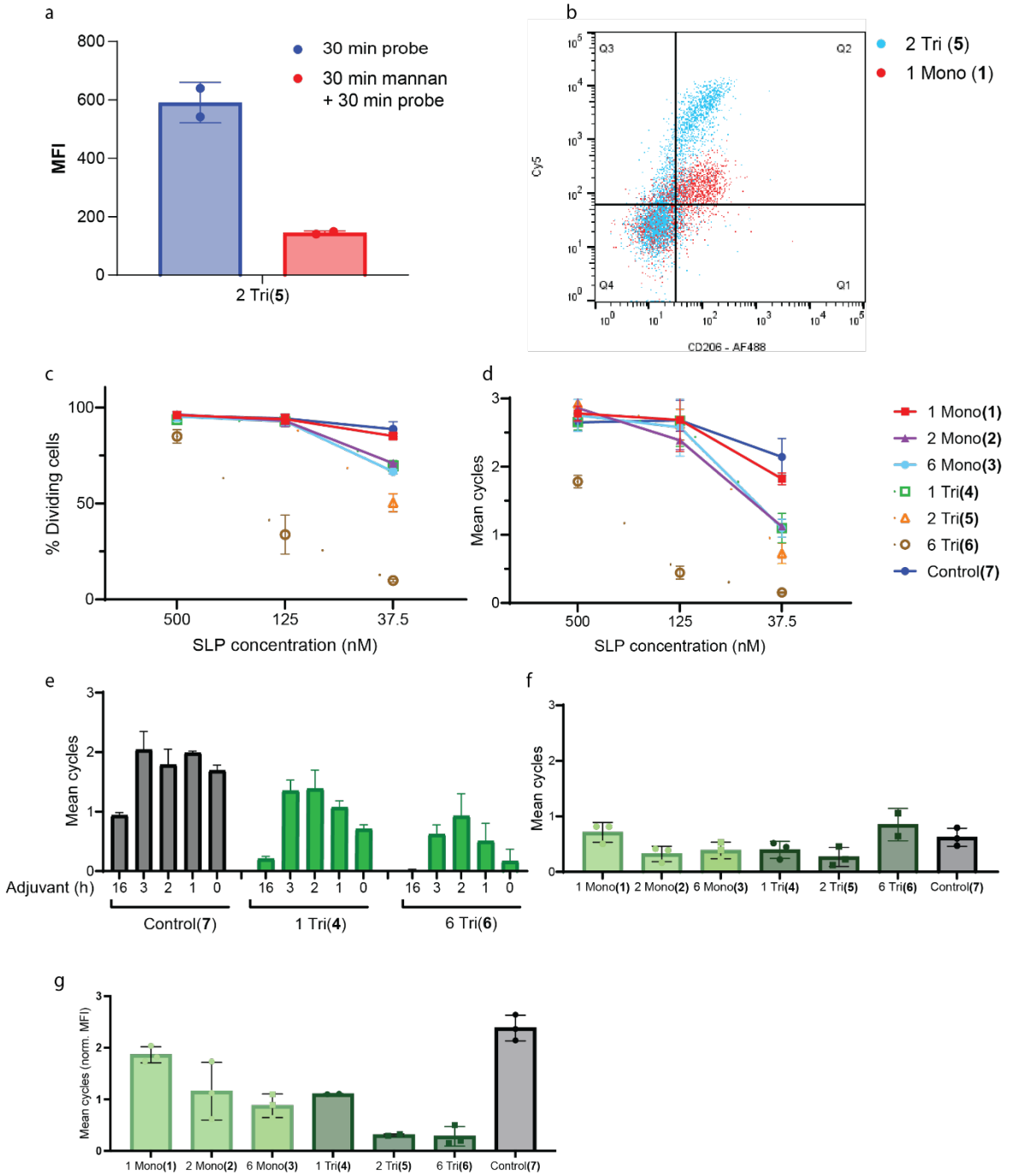

822
823 **Figure S8 | Uptake and cross-presentation of 1-7. A)** Endocytosis of **4** is blocked by pre-incubation of
824 BMDC with 2 mg/mL mannan for 30 min. **B)** Mannosylated antigens **1** and **4** are taken up by CD11c^{+}MR^{+}
825 BMDC. **C-D)** Cross-presentation by BMDC pulsed with different concentrations of antigen **1-7**. Amounts
826 of cross-presentation were determined by flow cytometric measurement of CFSE-dilution by
827 proliferating cognate T cells and quantified using mean cycle or percentage dividing cells of DMSO. **E)**
828 Pretreatment of BMDC with 1 µg/mL MPLA for indicated time before 2h pulse with antigen **1-7** and 3d
829 coculture with OT-I cells. **F**, Cross-presentation of antigens **1-7** by magnetically purified splenic DC. **G**,
830 Cross-presentation of immature BMDC pulsed with SLPs **1-7**

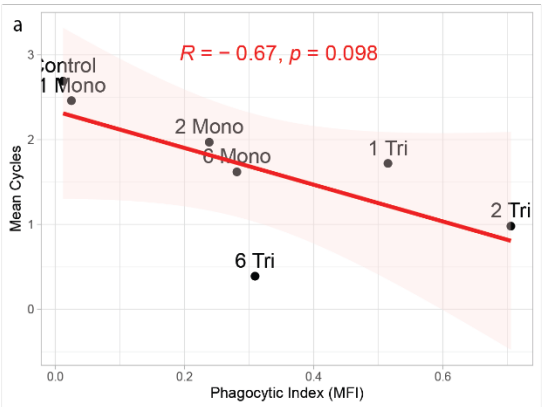

Figure S9 | Correlation between phagocytic index and cross-presentation of SLP 1-7 by BMDC. Pearson's R and two-tailed t test P value are displayed in the correlation plots.

Table S2 | Correlation analysis of uptake and cross-presentation with Glyco-PAINT-App derived kinetic parameters. (Absolute) Pearson's R and two-tailed t test P values are listed for each combination. Correlations presented in **Figure 4G-H** are highlighted in yellow and blue respectively.

Variable	Correlation _with_mean_cycle	Correlation_with_PI	Abs_Correlation _with_mean_cycle	Abs_Correlation _with_PI
Tau_E_BMDC_None	0.896	-0.611	0.896	0.611
AvgDC_E_BMDC_None	0.82	-0.946	0.82	0.946
MaxSpeed_E_BMDC_CytD	-0.699	0.731	0.699	0.731
AvgLongTrack_E_BMDC_None	-0.668	0.515	0.668	0.515
AvgLongTrack_E_BMDC_CytD	-0.538	0.3	0.538	0.3
AvgSpeed_E_BMDC_None	0.402	-0.785	0.402	0.785
KdSPR	0.399	-0.459	0.399	0.459
Density_E_BMDC_CytD	0.389	-0.383	0.389	0.383
MaxSpeed_E_BMDC_None	0.289	-0.855	0.289	0.855
Tau_E_BMDC_CytD	0.255	0.36	0.255	0.36
TotalTrack_E_BMDC_None	-0.247	-0.067	0.247	0.067
AvgSpeed_E_BMDC_CytD	-0.216	0.62	0.216	0.62
AvgShortTrack_E_BMDC_None	0.213	0.343	0.213	0.343
AvgShortTrack_E_BMDC_CytD	0.097	0.402	0.097	0.402
Density_E_BMDC_None	0.089	-0.627	0.089	0.627
AvgDC_E_BMDC_CytD	0.021	0.692	0.021	0.692
TotalTrack_E_BMDC_CytD	-0.02	0.298	0.02	0.298

RESOURCE AVAILABILITY

Lead contact

Further information and requests for resources and reagents should be directed to and will be fulfilled by the lead contact, Sander van Kasteren (s.i.vankasteren@chem.leidenuniv.nl)

Materials availability

A library of glycosylated synthetic long peptide antigens was synthesized in this study. All are available from the lead contact upon reasonable request until stocks run out.

Data and code availability

All newly generated code related to processing of Glyco-PAINT recordings is available on GitHub: github.com/jjabakker/GlycoPaint-Pipeline

Any additional information required to reanalyze the data reported in this paper is available from the lead contact upon request.

EXPERIMENTAL MODEL DETAILS

Mice

Male C57Bl/6J and OT-I (C57BL/6-Tg(TcraTcrb)1100Mjb/J) mice were purchased from the Jackson Laboratory (CA, USA). The animals were bred and housed under specific pathogen-free conditions and provided with water and food ad libitum under a 12:12 day/night cycle. Mice ranging from 8 to 15 weeks old were euthanized by cervical dislocation before harvest of lymphoid organs and/or thigh bones, femur, and tibia. All animal experiments received approval from the Dutch Central Authority for Scientific Procedures on Animals (CCD) on license number AVD1060020198832 and were conducted in accordance with the European Union Directive 2010/63/EU, recommendation 2007/526/EC.

Cell culture

Bone Marrow-Derived Dendritic Cells (BMDC)

Bone marrow (BM) was isolated from femurs, tibias, and thigh bones of C57Bl/6J mice via centrifugation (1900 *rcf*, 4.5 min) of scissor-cut bones that were placed in a 1.5 mL tube. The resulting pellet was subjected to red blood cell (RBC) lysis by resuspending in 0.5 mL of ammonium chloride-potassium (ACK) lysis buffer (Gibco, A1049201). After 3 min incubation at rt, the suspension was filtered over a 70 µm filter (Falcon, 352350), rinsed with 5 mL PBS and washed once with PBS by 5 min centrifugation at 300 *rcf* at rt. Thus obtained BM was resuspended at 1E6 cells / mL in 15 cm uncoated culture dishes (Sarstedt, 82.1184.500) in complete RPMI-1640 (Capricorn, RPMI-A) supplemented with 10% heat-inactivated fetal calf serum (FCS, Gibco, A5670701), penicillin (100 I.U./mL) & streptomycin (50 µg/mL) (Gibco, 15140148), 2 mM GlutaMAX (Gibco, 35050061), 50 µM 2-mercaptoethanol (Gibco, 31350010) and 20 ng/mL mGM-CSF (Peprotech, 315-03) and cultured in a humidified incubator at 37 °C and 5% CO2. On day two, 5mL of the above-described fresh medium was added and on day four cells were reseeded in fresh medium at 1E6/mL. Cells were used for microscopy and T cell activation experiments on day 7 or 8.

Bone Marrow-Derived Macrophages (BMDM)

Bone marrow (BM) was isolated from femurs, tibias, and thigh bones of C57Bl/6J mice via centrifugation (1900 *rcf*, 4.5 min) of scissor-cut bones that were placed in a 1.5 mL tube. The resulting pellet was subjected to red blood cell (RBC) lysis by resuspending in 0.5 mL of ACK lysing buffer (Gibco, A1049201). After 3 min incubation at rt, the suspension was filtered over a 70 µm filter (Falcon,

352350), rinsed with 5 mL PBS and washed once with PBS by 5 min centrifugation at 300 *rcf* at rt. Thus obtained BM was resuspended at 0.8E6 cells/mL in 15 cm uncoated culture dishes (Sarstedt, 82.1184.500) in complete RPMI-1640 (Capricorn, RPMI-A) supplemented with 10% heat-inactivated fetal calf serum (FCS, Gibco, A5670701), penicillin (100 I.U./mL) & streptomycin (50 µg/mL) (Gibco, 15140148), 2 mM GlutaMAX (Gibco, 35050061), 50 µM 2-mercaptoethanol (Gibco, 31350010) and 20 20 ng/mL M-CSF (Biolegend, 576404) and cultured in a humidified incubator at 37°C and 5% CO_2. On day 2, 5 mL fresh medium was added and on day 4 medium was aspirated and replenished with 15 mL fresh medium. Cells were used for experiments on day 7 or 8.

CHO-MR

The CHO-MR cell line was kindly provided by Luisa Martinez-Pomares[3] and cultured in DMEM/F12 without phenol red (Gibco, 21041025), supplemented with 10% FCS, penicillin (100 I.U./mL), streptomycin (50 µg/mL) and selection antibiotic G418 (0.6 mg/mL). A layer of adherent cells was washed with PBS and cells were harvested by 10 min incubation with 2 mM EDTA in PBS and subcultured approximately twice per week at a 1:5 split when cells reached 70-80% confluency.

EXPERIMENTAL METHOD DETAILS

Statistical analysis and sample size

Statistical analyses were conducted to compare glycan ligand binding kinetics across probes using the Glyco-PAINT square-based subsampling technology. Subsampling subcellular regions (squares) within fields of view increased the number of independent data points, enhancing statistical power compared to treating entire fields of view or cells as single units. For all Glyco-PAINT experiments at least 5 biological replicates (independent experiments with fresh mouse material or new passage number for cell lines) with 3 technical replicates (fields of view per condition) were recorded. For flow cytometry assays at least 3 biological replicates with 2 technical replicates per condition were conducted. A two-way ANOVA was used to assess differences among probes with respect to kinetic parameters derived from Glyco-PAINT experiments and flow cytometric assays, followed by Tukey's Honest Significant Difference (HSD) test for post-hoc comparisons to control Type I error. Significance is reported as: ns (not significant), $p \geq 0.05$; $p < 0.05$ (*); $p < 0.01$ (**); $p < 0.001$ (***); and $p < 0.0001$ (****).

Fluorescent glycan probes

Glycan and glycan SLP probes were stored as lyophilized powders at -20°C. Upon thawing, vials were reconstituted in DMSO and concentration was determined by measurement of absorbance using Nanodrop apparatus with extinction coefficients e_{sCy5} = 250.000 $M^{-1}cm^{-1}$ at 641 nm and $e_{ATTO655}$ = 125.000 $M^{-1}cm^{-1}$ at 663 nm. Small aliquots were stored at -20 °C until use.

OT-I T cell isolation

A 70 µm filter was placed on a 50 mL tube and pre-wetted with PBS supplemented with 2 mM EDTA and 2% FCS (single-cell suspension buffer, SCSB). Freshly harvested spleens from OT-I transgenic mice were placed on the filter and disrupted with the back end of a syringe. After thorough washing, the suspension was centrifuged (10 min., 300 *rcf*, rt). Next, the pellet was gently resuspended in 2 mL of ACK lysing buffer (Gibco, A1049201). After 3 min incubation the suspension was diluted with 10 mL PBS, filtered once more, and centrifuged again (300 *rcf*, 10 min, rt). The pellet was resuspended and subjected to magnetically-activated depletion of non-target cells using the "Naïve CD8a+ T cell isolation Kit" (Miltenyi, 130-096-543) according to manufacturer's protocol. The obtained T cells were counted and resuspended at a density of 5-15E6 / mL in 1 mL PBS with 5 µM CFSE (Biolegend) and incubated for 15 min. at 37 °C. After incubation, cells were spun down (10 min, 300 rcf, rt), washed once more with complete RPMI-1640 and were ready for downstream use.

934 **Splenic DC isolation**
935 Spleens isolated from C57Bl/6J mice were placed on a 10 cm petri dish (Sarstedt, 83.3902) containing
936 5 mL HBSS (Gibco, 14025092) supplemented with 1 mg/mL collagenase IV (Sigma, NC2115693) and
937 20 U/mL DNAse (Thermo Scientific, EN0525) and minced into small pieces. After incubating for 30 min
938 at 37 °C, tissue digestion was stopped by addition of 2 mM EDTA. The remaining homogenate was
939 disrupted and RBC-lysed as described above and subjected to magnetically-activated depletion of non-
940 target cells using the "Pan Dendritic Cell isolation Kit" (Miltenyi, 130-100-875) according to
941 manufacturer's protocol.
942
943 **Glycan uptake experiments**
944 2.5E5 BMDC or CHO-MR were seeded in a 96 well v-bottom plate (Sarstedt, 82.1583001). The next
945 day, Glycan SLP probes were added to the cells at 250 nM and incubated for 1h at 37 °C. Active uptake
946 was halted by addition of ice-cold PBS and washed twice (300 *rcf*, 5 min., rt). Cells were stained with
947 Zombie Yellow (Biolegend, 423103, 1:500), TruStain FcX (Biolegend, 101319, 1:100), CD11c -
948 eFluor450 (clone: N418, eBioscience, 48-0114-82**,** 1:200), CD206-AF488 (clone: MR5D3, Biorad,
949 MCA2235A488T, 1:20), acquired on Guava EasyCyte 12HT and analyzed using FlowJo v8. Phagocytic
950 index (PI) was calculated according to equation 1. Statistical analysis and plotting were performed
951 using GraphPad Prism V10.
952
953 $PI = \%\ sCy5^{+}\ cells \times MFI\ sCy5^{+}\ cells - \%\ sCy5^{-}\ cells \times MFI\ sCy5^{-}\ cells$ (eq. 1)
954
955 **T cell proliferation assay**
956 5E4 BMDC or 1E5 splenic DC were seeded in 96 well Nunc U-bottom plates (Thermo Scientific, 168136)
957 and pulsed with Glycan SLP at 40 nM for indicated time. In indicated experiments, DC were pretreated
958 with 1 µg/mL MPLA (Avanti, 699800P) for 2h before antigen pulse. After antigen pulse was finished,
959 the plate was spun down for 3 min at 600 *rcf*, washed once with complete RPMI-1640 and 1-1.5E5
960 freshly isolated, CFSE-stained OT-I T cells were added to the pulsed DCs in 200 µL complete RPMI-1640
961 and incubated at 37 °C. After 3d of coculture, the plate was spun down (3 min, 600 rcf, 4 °C) and
962 supernatant was removed and stored at -80°C. Cells were washed with FACS buffer (PBS with 2 mM
963 EDTA, 2% FCS and 7.4 mM NaN3) and stained with Aqua Live/DEAD (Invitrogen, L34957, 1:500),
964 TruStain FcX (Biolegend, 101319, 1:100), CD8a - APC (clone: 53-7.6, Biolegend, 100711, 1:200), and
965 TCR V beta 5.1/5.2 - eFluor450 (clone: MR9-4, eBioscience, 48-5796-82) for 30 min on ice, washed two
966 times and acquired on a BD Fortessa I flow cytometer and analyzed using FlowJo v8. To calculate mean
967 cycle, the CFSE dilution factor was obtained by dividing the MFI of the antigen pulsed condition by the
968 DMSO pulsed condition expressed as Log2.[4] Statistical analysis and plotting was performed using
969 GraphPad Prism V10.
970
971 **BMDM polarization**
972 At day 6 adherent macrophages were harvested by aspiration of medium, washing once with PBS and
973 incubation with 10 mL of 2 mM EDTA in PBS for 10 min at 37°C. Cells were reseeded in complete
974 medium with addition of polarizing stimulus, 20 ng/mL IFN-γ (Peprotech, 315-05-100UG) + 100 ng/mL
975 LPS-EB (Invivogen, tlrl-eblps) for M1 or 20 ng/mL IL-4 (Peprotech, 214-14-20UG) for M2 for 16h.
976
977 **Optical setup**
978 Single molecule imaging was performed on a Nikon Ti2 N-STORM system equipped with TIRF module,
979 Z piezo element, perfect focus system for axial drift correction and an OkoLab incubator with
980 temperature and CO2 controller (37 °C and 5% CO2) for live-cell imaging. Recordings were acquired
981 using the 647 nm excitation laser (160 mW, 1.9 kW/cm2). Upon laser excitation, fluorescence was
982 collected by a 100x 1.49 NA oil-immersion objective, passed through a quad-band dichroic mirror
983 (97335 Nikon), and detected by a Hamamatsu ORCA Flash 4.0 CMOS camera with 160 nm pixel size.
984 The signal was collected using the following settings: 512x512 pixel region, no binning, pixel depth 16-

bit, exposure time 50 ms, live-cell observation and 2D-STORM (lens out), zoom 1x, lens x0.4 and for live-cell observation at 37°C the correction collar was set to position 8160.

Acquisition of Glyco-PAINT recordings

5E4 CHO-MR or 1E5 BMDC were seeded in 8 well glass-bottomed microscopy slides (Ibidi, 80827) in complete medium. After equilibration in the microscope incubator, fluorescent glycan was added at 5 nM for CHO-MR and 10 nM for BMDC experiments. Then, cells were brought into focus using brightfield illumination and 2,000 frames (at 50 ms intervals) were recorded within a single field-of-view at 40-60% of maximum 647 nm laser power using TIRF illumination. For indicated experiments, Cytochalasin D (Focus Biomolecules) was added to a final concentration of 10 µM for 30 min prior to acquisition.

ROI-based analysis of Glyco-PAINT recordings

TrackMate was run manually using the Fiji plugin.[5] The LoG spot detection algorithm was applied with an object radius of 0.5 µm, with pre-processing with median filter and sub-pixel localization unchecked. Threshold values were set to 5, 10 or 15 such that no more than 800.000 spots were detected and kept identical per experimental condition. Next, single-particle tracking was performed using the Simple LAP tracker algorithm with a maximum frame gap of 3, a max linking distance of 0.6 µm and a gap closing max distance of 1.2 µm. Tracks with only two spots were discarded. Then, manual Regions of Interest (ROIs) were drawn in individual recordings using Fiji based on brightfield-defined cell outlines. The number of tracks residing within the ROI were compared with the number of tracks outside the ROI to establish a ratio of cell / glass density. Only recordings for which that ratio exceeded 2 were considered for further analysis. For all remaining recordings, the k_{on}, k_{off} and MSD were calculated for tracks within the ROI according to the procedure as described by Riera et al.[1] Statistical analysis and plotting was performed using GraphPad Prism v10.

Glyco-PAINT-APP analysis of recordings

Processing of recordings using Glyco-PAINT-APP was performed as described in a step-by-step procedure in the **Supplementary Manual** and accompanying **Supplementary Videos 1 and 2**. For the TrackMate processing, a batch file (Experiment Info.csv) containing the experiment metadata and tracking parameters was created. Threshold values were set to 5, 10 or 15 such that no more than 800.000 spots were detected and kept identical per experimental condition. Recordings were then processed in TrackMate using the 'Run TrackMate Batch' plugin provided by the Glyco-PAINT-APP. Through this plugin, spot detection and tracking by TrackMate[5] was performed as indicated in the batch file using the Simple LAP tracker algorithm with a maximum frame gap of 3, a max linking distance of 0.6 µm and a gap closing max distance of 1.2 µm. Tracks with only two spots were discarded.

With the Glyco-PAINT-APP utility 'Generate Squares', a grid of squares was overlaid and kinetic properties for each square were calculated. Default parameters for grid processing are (deviations are mentioned in figure captions): Nr of Squares in row 20, Minimum Tracks to Calculate Tau 20, Min allowable R Squared 0.1, Min Required Density Ratio 2 and Maximum Allowable Variability 10.

For every recording, a background track count was calculated by averaging the track count of the 40 (10% of the total number of squares) least dense squares. Only squares for which the track count exceeded the Min Required Density Ratio of 2 were considered (and the remaining ignored as background). For each square also the variability was calculated and only squares for which the variability was less than the Maximum Allowable Variability of 10 were considered. For squares meeting both the Minimum Required Density Ratio and Maximum Allowable Variability criteria, and containing at least the Minimum Tracks to Calculate Tau kinetic parameters including k_{on}, k_{off} and MSD

1032 were calculated as in Riera et al.[1], or copied from the TrackMate Tracks table output (for velocity,
1033 displacement, and track duration).

1034 Summary files were created using the 'Compile Project' utility, creating an 'All Recordings.csv' file,
1035 containing information for all 973 recordings, an 'All Squares.csv' file containing information on
1036 389,200 (973 x 400) squares and an 'All Tracks.csv' file containing information on 13.4 mln tracks
1037 (binding events) in the project. Statistical analysis and plotting using these merged files was performed
1038 using the ggplot2 package in R.[6,7]

1039 **General procedure for automated SPPS**

1040 Peptides were synthesized using automated Fmoc-SPPS on a Liberty Blue[tm] automated microwave
1041 peptide synthesizer (CEM corporation). Synthesis was performed 100 µmol scale on Tentagel S RAM
1042 resin (loading 0.20-0.25 mmol/g, Rapp Polymere GmbH, Germany). Resin was first swollen for 5
1043 minutes in DMF prior to amino acid coupling. Activation was achieved using DIC/Oxyma coupling as
1044 recommended by the manufacturer. The following amino acids were used: Fmoc-Ala-OH, Fmoc-
1045 Arg(Pbf)-OH, Fmoc-Asn(Trt)-OH, Fmoc-Asp(OtBu)-OH, Fmoc-Gln(tBu)-OH, Fmoc-Glu(OtBu), Fmoc-Gly-
1046 OH, Fmoc-Ile-OH, Fmoc-Leu-OH, Fmoc-Lys(Boc)-OH, Fmoc-Lys(Mmt)-OH, Fmoc-Phe-OH, Fmoc-
1047 Ser(tBu)-OH, Fmoc-Val-OH. All amino acids were obtained from Novabiochem except Fmoc-Lys(Mmt)-
1048 OH which was obtained from CEM corporation. Standard coupling was achieved using 5 equivalents
1049 amino acid as a 0.2 M amino acid/DMF solution, 5 equivalents DIC as a 0.5 M of DIC/DMF solution and
1050 5 equivalents Oxyma as a 1 M Oxyma/DMF solution (also containing 0.2 M DiPEA), at 90°C for 2
1051 minutes. Standard Fmoc deprotection was achieved by 20% (v/v) piperidine in DMF at 90°C for 90
1052 seconds, repeated once. To analyze the quality of the peptide, a small amount of resin (~1mg) was
1053 treated with 200 µL of a TFA cocktail (95:2.5:2.5, TFA/H_2O/TIS) for 2 hours, after which the TFA was
1054 filtered into 800 µL of ice cold Et_2O. After five minutes the formed precipitate was collected by
1055 centrifugation and the supernatant discarded. The pellet was dissolved in 200 µL 1:1:1
1056 H_2O/MeCN/tBuOH and subjected to LC-MS analysis. Peptides were characterized using electrospray
1057 ionization mass spectrometry (ESI-MS) on a Thermo Finnigan LCQ Advantage Max LC-MS instrument
1058 with a Surveyor PDA plus UV detector on an analytical C18 column (Phenomenex, 3 µm, 110 Å, 50 mm
1059 × 4.6 mm) in combination with buffers A (H_2O), B (MeCN), and C (1% aq TFA). Quality of crude was
1060 evaluated with a linear gradient of 10-90% B with a constant 10% C over 10 minutes.

1061 **General procedures for manual SPPS**

1062 Manual elongation of peptides was carried out in a fritted syringe at either 25 or 5 µmol scale. Fmoc
1063 deprotection was achieved using 20 % (v/v) piperidine in DMF in two steps, reacting 3 and 7 minutes,
1064 respectively. Fmoc-Gly-OH was coupled using 5 equivalents of amino acid together with 5 equivalents
1065 of HCTU (as a 0.5 M solution) and 10 equivalents DiPEA for 45 minutes. Fmoc-Lys(N_3)-OH was coupled
1066 using 2 equivalents together with 2 equivalents HCTU (as a 0.2 M in DMF solution) and 4 equivalents
1067 of DiPEA for 90 minutes. Fmoc-TEG-OH was coupled using 4 equivalents, together with 4 equivalents
1068 HCTU and 8 equivalents DiPEA in 1 mL of DMF for 45 minutes. Analysis of the quality of the resin-
1069 bound peptide was carried out as above.

1070 **General procedure for *N*-terminal acetylation**

1071 The *N*-terminal Fmoc was cleaved by treating the resin twice with a 20% (v/v) solution of piperidine in
1072 DMF, for 3 and 7 minutes. This was followed by the addition of a solution containing 10 % (v/v) Ac_2O
1073 and 5 % (v/v) DiPEA in DMF (1 mL for 25 µmol resin bound peptide). This resin was acetylated for 15
1074 minutes under gentle agitation, followed by draining the acetylation solution and thorough washing
1075 of the resin with DMF.

1076 **General procedure for fluorophore labeling**
1077 Fluorophore labeling of peptides was carried out on a 5 µmol scale. The resin was first swelled in DCM,
1078 followed by selective Mmt deprotection. The Mmt group protecting the C-terminal lysine residue, the
1079 resin was treated with a mildly acidic mixture consisting of 10 % (v/v) AcOH and 20 % (v/v) TFE in DCM
1080 (1 mL) for one hour[8]. After this time has elapsed, the resin was washed three times with DCM and
1081 three times with DMF. To remove residual acetic acid, the resin was then treated with a 10 % TEA in
1082 DMF mixture (2 x 10 min) followed by an additional three washes with DMF. One equivalent of
1083 fluorophore was dissolved in a 50 mM solution of HCTU together with 2 equivalents of DiPEA. This
1084 mixture was added to the drained resin and allowed to react under gentle agitation overnight
1085 protected from light. After overnight coupling the solution was drained and the resin was thoroughly
1086 washed with DMF.

1087 **General procedure for peptide global deprotection and purification**
1088 Peptide cleavage was carried out using a standard TFA cleavage cocktail (TFA:H_2O:TIS 95:2.5:2.5) using
1089 1 mL per 25 µmol of resin bound peptide. Before initiating cleavage, the resin was thoroughly washed
1090 with DCM and drained. The TFA cocktail was added and mixed with the resin under gentle agitation
1091 for one hour, after which it was drained into a centrifuge tube containing ice cold diethyl ether (10:1
1092 ratio Et_2O:TFA). When deprotecting fluorophore modified peptides, the cleavage reaction was
1093 protected from light as much as possible and a 20:1 ratio of Et_2O to TFA was used. The
1094 diethylether/TFA mixture was chilled for a minimum of 10 minutes to increase peptide recovery, and
1095 the precipitated peptide was recovered by centrifugation. The supernatant was discarded and the
1096 pellet washed with a small amount of Et_2O, followed again by centrifugation. This pellet was dissolved
1097 in a mixture of H_2O:MeCN:tBuOH and subjected to RP-HPLC purification on a Gilson GX281
1098 semipreparative HPLC. This machine was equipped with a Gemini-NX C18 column (5 µm, 110 A, 250 x
1099 10.0 mm) using a flow of 5 mL/min and buffers A = 0.1% TFA in H_2O and B = MeCN. Peak detection
1100 was done using a UV-Vis detector set to 225 nm or 610 nm for fluorescently labeled peptides. Quality
1101 of purified peptides was determined using an electrospray ionization mass spectrometry (ESI-MS) on
1102 a Thermo Finnigan LCQ Advantage Max LC-MS instrument with a Surveyor PDA plus UV detector on
1103 an analytical C18 column (Phenomenex, 3 µm, 110 Å, 50 mm × 4.6 mm) in combination with buffers A
1104 (H_2O), B (MeCN), and C (1% aq TFA). Quality of the peptides was evaluated with a linear gradient of
1105 10-50% B with a constant 10% C over 9 minutes or a linear gradient of 10-90% B with a constant 10%
1106 C over 9 minutes.

1107 **Fmoc-Lys(N_3)-Lys(N_3)-Lys(N_3)-Lys(N_3)-Lys(N_3)-Lys(N_3)-TEG-Asp(OtBu)-Glu(OtBu)-Val-Ser(tBu)-Gly-**
1108 **Leu-Glu(OtBu)-Gln(Trt)-Leu-Glu(OtBu)-Ser(tBu)-Ile-Ile-Asn(Trt)-Phe-Glu(OtBu)-Lys(Boc)-Leu-Ala-**
1109 **Ala-Ala-Ala-Ala-Lys(Mmt)-RAM-Tentagel S (18)**
1110 Resin bound peptide **16** (25 µmol) was elongated manually with Fmoc-TEG-OH and Fmoc-Lys(N_3)-OH.
1111 **LC-MS** RT = 7.6 min (C18, 10-90% B over 9 minutes) **LRMS** calcd $[M+2H]^{2+}$ = 1941.52, $[M+3H]^{3+}$ =
1112 1294.68 observed M/z = 1941.53, 1294.80

1113 **Ac-Lys(N_3)-Lys(N_3)-Lys(N_3)-Lys(N_3)-Lys(N_3)-Lys(N_3)-TEG-Asp-Glu-Val-Ser-Gly-Leu-Glu-Gln-Leu-Glu-**
1114 **Ser-Ile-Ile-Asn-Phe-Glu-Lys-Leu-Ala-Ala-Ala-Ala-Ala-Lys(sCy5)-NH_2 (19)**
1115 Resin bound peptide **18** (5 µmol) was N-terminally acetylated according to the standard conditions.
1116 This was followed by chemoselective deprotection of the Mmt group and coupling of sCy5-OH (1.0 eq,
1117 3.2 mg, 5 µmol) as described in the general methods. Global deprotection followed by RP-HPLC
1118 purification yielded compound **19** as a blue solid (1.60 mg, 0.37 µmol, 7.4%). **LC-MS** RT = 6.0 min (C18,
1119 10-90% B over 9 minutes) **LRMS** calcd $[M+3H]^{3+}$ = 1443.06 observed M/z = 1443.00

Fmoc-Lys(N_3)-Gly-Lys(N_3)-TEG-Asp(OtBu)-Glu(OtBu)-Val-Ser(tBu)-Gly-Leu-Glu(OtBu)-Gln(Trt)-Leu-Glu(OtBu)-Ser(tBu)-Ile-Ile-Asn(Trt)-Phe-Glu(OtBu)-Lys(Boc)-Leu-Ala-Ala-Ala-Ala-Ala-Lys(Mmt)-RAM-Tentagel S (20)

Resin bound peptide **22** (25 µmol) was elongated manually with Fmoc-TEG-OH, Fmoc-Lys(N_3)-OH and Fmoc-Gly-OH. **LC-MS** RT = 6.5 min (C18, 10-90% B over 9 minutes) **LRMS** calcd $[M+2H]^{2+}$ = 1661.86, $[M+3H]^{3+}$ = 1108.24 observed M/z = 1662.00, 1108.67

Ac-Lys(N_3)-Gly-Lys(N_3)-TEG-Asp-Glu-Val-Ser-Gly-Leu-Glu-Gln-Leu-Glu-Ser-Ile-Ile-Asn-Phe-Glu-Lys-Leu-Ala-Ala-Ala-Ala-Ala-Lys(sCy5)-NH_2 (21)

Resin bound peptide **20** (5 µmol) was N-terminally acetylated according to the standard conditions. This was followed by chemoselective deprotection of the Mmt group and coupling of sCy5-OH (1.0 eq, 3.2 mg, 5 µmol) as described in the general methods. Global deprotection followed by RP-HPLC purification yielded compound **21** as a blue solid (1.24 mg, 0.33 µmol, 6.6%). **LC-MS** RT = 5.0 min (C18, 10-90% B over 9 minutes) **LRMS** calcd $[M+2H]^{2+}$ = 1883.93, $[M+3H]^{3+}$ = 1256.28 observed M/z = 1884.42, 1256.67

Ac-Lys(N_3)-TEG-Asp(OtBu)-Glu(OtBu)-Val-Ser(tBu)-Gly-Leu-Glu(OtBu)-Gln(Trt)-Leu-Glu(OtBu)-Ser(tBu)-Ile-Ile-Asn(Trt)-Phe-Glu(OtBu)-Lys(Boc)-Leu-Ala-Ala-Ala-Ala-Ala-Lys(Mmt)-RAM-Tentagel S (22)

Resin bound peptide **16** (25 µmol) was elongated manually with Fmoc-TEG-OH, Fmoc-Lys(N_3)-OH and Fmoc-Gly-OH, followed by acetylation under standard conditions. **LC-MS** RT = 4.9 min (C18, 10-90% B over 9 minutes) **LRMS** calcd $[M+2H]^{2+}$ = 1465.77, $[M+3H]^{3+}$ = 977.51 observed M/z = 1466.33, 977.83

Ac-Lys(N_3)-TEG-Asp-Glu-Val-Ser-Gly-Leu-Glu-Gln-Leu-Glu-Ser-Ile-Ile-Asn-Phe-Glu-Lys-Leu-Ala-Ala-Ala-Ala-Ala-Lys(sCy5)-NH_2 (23)

Resin bound peptide **22** (5 µmol) was chemoselectively deprotected to remove the Mmt group, followed by coupling of sCy5-OH (1.0 eq, 3.2 mg, 5 µmol) as described in the general methods. Global deprotection followed by RP-HPLC purification yielded compound **23** as a blue solid (0.88 mg, 0.25 µmol, 4.9%). **LC-MS** RT = 4.7 min (C18, 10-90% B over 9 minutes) **LRMS** calcd $[M+2H]^{2+}$ = 1777.87, $[M+3H]^{3+}$ = 1185.58 observed M/z = 1778.67, 1186.08

Ac-TEG-Asp-Glu-Val-Ser-Gly-Leu-Glu-Gln-Leu-Glu-Ser-Ile-Ile-Asn-Phe-Glu-Lys-Leu-Ala-Ala-Ala-Ala-Ala-Lys(sCy5)-NH_2 (7)

Resin bound peptide **16** (25 µmol) was elongated manually with Fmoc-TEG-OH followed by N-terminal acetylation according to the standard conditions. Next, chemoselective deprotection of the Mmt group and coupling of sCy5-OH (1.0 eq, 3.2 mg, 5 µmol) as described in the general methods yielded the fully protected, resin bound peptide. Global deprotection followed by RP-HPLC purification yielded compound **7** as a blue solid (1.44 mg, 0.42 µmol, 8.5%). **LC-MS** RT = 4.6 min (C18, 10-90% B over 9 minutes) **LRMS** calcd $[M+2H]^{2+}$ = 1701.32, $[M+3H]^{3+}$ = 1134.54 observed M/z = 1701.58, 1134.75

CuAAC glycopeptide conjugation

General procedures for CuAAC modification of peptides

Peptides were dissolved in degassed DMSO and glycans in either degassed DMSO or degassed MilliQ water. These were mixed in a 1.5 mL Eppendorf tube, followed by addition of a copper click mix. This click mix typically consistent of 1 part 0.1 M $CuSO_4$ (in MQ), 2 parts 0.1 M sodium ascorbate (in MQ) and 3 parts 0.1 M THPTA (in DMSO), giving a solution with a total Cu(I) concentration of around 15 mM. Of this solution, enough was added to be 0.15 equivalents compared to the peptide. The reaction was heated in a 40°C shaker block, and every 24 hours 1 equivalent of 0.1 M sodium ascorbate was added. Periodically, a 0.5 µL sample was diluted into 39.5 µL of 1:1:1 H_2O:MeCN:tBuOH and analyzed by LC-MS to evaluate reaction progression. After full conversion of the peptide towards the desired

conjugate was observed, the reaction mixture was subjected to size exclusion chromatography over Toyopearl HW-40 size exclusion resin using 150 mM NH_4OAc or 150 mM NH_4HCO_3 (containing 20% MeCN) as the buffer. Fractions showing absorbance at 610 nm were combined and lyophilized.

Ac-Lys(Man)-Lys(Man)-Lys(Man)-Lys(Man)-Lys(Man)-Lys(Man)-TEG-Asp-Glu-Val-Ser-Gly-Leu-Glu-Gln-Leu-Glu-Ser-Ile-Ile-Asn-Phe-Glu-Lys-Leu-Ala-Ala-Ala-Ala-Ala-Lys(sCy5)-NH_2 (3)
Compound **19** (100 nmol, 50 mM in DMSO) was mixed with propargyl mannoside **14** (12 eq., 6 µL of 200 mM solution in DMSO). 1 µL of the standard click mix was added and the reaction carried out at 40°C. After SEC purification and lyophilization compound **3** was obtained as a blue powder (0.48 mg, 85 nmol, 85%). **LC-MS** RT = 4.3 min (C18, 10-50% B over 9 minutes) **LRMS** calcd $[M+3H]^{3+}$ = 1879.21, $[M+4H]^{4+}$ = 1409.66 observed M/z = 1879.33, 1409.83

Ac-Lys(triMan)-Lys(triMan)-Lys(triMan)-Lys(triMan)-Lys(triMan)-Lys(triMan)-TEG-Asp-Glu-Val-Ser-Gly-Leu-Glu-Gln-Leu-Glu-Ser-Ile-Ile-Asn-Phe-Glu-Lys-Leu-Ala-Ala-Ala-Ala-Ala-Lys(sCy5)-NH_2 (6)
Compound **19** (100 nmol, 50 mM in DMSO) was mixed with propargyl mannoside **15** (12 eq., 6 µL of 200 mM solution in DMSO). 1 µL of the standard click mix was added and the reaction carried out at 40°C. After SEC purification and lyophilization compound **6** was obtained as a blue powder (0.41 mg, 54 nmol, 54%). **LC-MS** RT = 4.2 min (C18, 10-50% B over 9 minutes) **LRMS** calcd $[M+4H]^{4+}$ = 1896.07, $[M+5H]^{5+}$ = 1517.06 observed M/z = 1896.08, 1517.17

Ac-Lys(Man)-Gly-Lys(Man)-TEG-Asp-Glu-Val-Ser-Gly-Leu-Glu-Gln-Leu-Glu-Ser-Ile-Ile-Asn-Phe-Glu-Lys-Leu-Ala-Ala-Ala-Ala-Ala-Lys(sCy5)-NH_2 (2)
Compound **21** (100 nmol, 25 mM in DMSO) was mixed with propargyl mannoside **14** (4 eq., 2 µL of 200 mM solution in DMSO). 1 µL of the standard click mix was added and the reaction carried out at 40°C. After SEC purification and lyophilization compound **2** was obtained as a blue powder (0.25 mg, 60 nmol, 60%). **LC-MS** RT = 6.8 min (C18, 10-50% B over 9 minutes) **LRMS** calcd $[M+3H]^{3+}$ = 1402.00 observed M/z = 1402.08

Ac-Lys(triMan)-Gly-Lys(triMan)-TEG-Asp-Glu-Val-Ser-Gly-Leu-Glu-Gln-Leu-Glu-Ser-Ile-Ile-Asn-Phe-Glu-Lys-Leu-Ala-Ala-Ala-Ala-Ala-Lys(sCy5)-NH_2 (5)
Compound **21** (100 nmol, 25 mM in DMSO) was mixed with propargyl mannoside **15** (4 eq., 2 µL of 200 mM solution in DMSO). 1 µL of the standard click mix was added and the reaction carried out at 40°C. After SEC purification and lyophilization compound **5** was obtained as a blue powder (0.29 mg, 60 nmol, 60%). **LC-MS** RT = 6.6 min (C18, 10-50% B over 9 minutes) **LRMS** calcd $[M+3H]^{3+}$ = 1618.07 observed M/z = 1618.08

Ac-Lys(Man)-TEG-Asp-Glu-Val-Ser-Gly-Leu-Glu-Gln-Leu-Glu-Ser-Ile-Ile-Asn-Phe-Glu-Lys-Leu-Ala-Ala-Ala-Ala-Ala-Lys(sCy5)-NH2 (1)
Compound **23** (100 nmol, 25 mM in DMSO) was mixed with propargyl mannoside **14** (2 eq., 1 µL of 200 mM solution in DMSO). 1 µL of the standard click mix was added and the reaction carried out at 40°C. After SEC purification and lyophilization compound **1** was obtained as a blue powder (0.30 mg, 79 nmol, 79%). **LC-MS** RT = 4.4 min (C18, 10-90% B over 9 minutes) **LRMS** calcd $[M+2H]^{2+}$ = 1886.91, $[M+3H]^{3+}$ = 1258.27 observed M/z = 1887.33, 1258.75

Ac-Lys(triMan)-TEG-Asp-Glu-Val-Ser-Gly-Leu-Glu-Gln-Leu-Glu-Ser-Ile-Ile-Asn-Phe-Glu-Lys-Leu-Ala-Ala-Ala-Ala-Ala-Lys(sCy5)-NH_2 (4)
Compound **23** (100 nmol, 25 mM in DMSO) was mixed with propargyl mannoside **15** (2 eq., 1 µL of 200 mM solution in DMSO). 1 µL of the standard click mix was added and the reaction carried out at 40°C. After SEC purification and lyophilization compound **4** was obtained as a blue powder (0.26 mg,

63 nmol, 63%). **LC-MS** RT = 4.4 min (C18, 10-90% B over 9 minutes) **LRMS** calcd $[M+3H]^{3+}$ = 1366.31 observed M/z = 1366.75

REFERENCES

(1) Riera, R.; Hogervorst, T. P.; Doelman, W.; Ni, Y.; Pujals, S.; Bolli, E.; Codée, J. D. C.; van Kasteren, S. I.; Albertazzi, L. Single-Molecule Imaging of Glycan–Lectin Interactions on Cells with Glyco-PAINT. *Nat Chem Biol* **2021**, *17* (12), 1281–1288. https://doi.org/10.1038/s41589-021-00896-2.

(2) Li, R.-J. E.; Hogervorst, T. P.; Achilli, S.; Bruijns, S. C.; Arnoldus, T.; Vivès, C.; Wong, C. C.; Thépaut, M.; Meeuwenoord, N. J.; van den Elst, H.; Overkleeft, H. S.; van der Marel, G. A.; Filippov, D. V.; van Vliet, S. J.; Fieschi, F.; Codée, J. D. C.; van Kooyk, Y. Systematic Dual Targeting of Dendritic Cell C-Type Lectin Receptor DC-SIGN and TLR7 Using a Trifunctional Mannosylated Antigen. *Front. Chem.* **2019**, *7*, 650. https://doi.org/10.3389/fchem.2019.00650.

(3) Su, Y.; Bakker, T.; Harris, J.; Tsang, C.; Brown, G. D.; Wormald, M. R.; Gordon, S.; Dwek, R. A.; Rudd, P. M.; Martinez-Pomares, L. Glycosylation Influences the Lectin Activities of the Macrophage Mannose Receptor. *Journal of Biological Chemistry* **2005**, *280* (38), 32811–32820. https://doi.org/10.1074/jbc.M503457200.

(4) *Apoptotic cell capture by DCs induces unexpectedly robust autologous CD4+ T-cell responses - Valente - 2014 - European Journal of Immunology - Wiley Online Library*. https://onlinelibrary.wiley.com/doi/full/10.1002/eji.201344191 (accessed 2024-12-23).

(5) *TrackMate 7: integrating state-of-the-art segmentation algorithms into tracking pipelines | Nature Methods*. https://www.nature.com/articles/s41592-022-01507-1 (accessed 2024-07-26).

(6) Wickham, H. *Ggplot2: Elegant Graphics for Data Analysis*; Springer-Verlag New York, 2016.

(7) R Core Team. *R: A Language and Environment for Statistical Computing*; R Foundation for Statistical Computing: Vienna, Austria, 2023.

(8) Aletras, A.; Barlos, K.; Gatos, D.; Koutsogianni, S.; MAMOS, P. Preparation of the Very Acid-sensitive Fmoc-Lys(Mtt)-OH Application in the Synthesis of Side-chain to Side-chain Cyclic Peptides and Oligolysine Cores Suitable for the Solid-phase Assembly of MAPs and TASPs. *International Journal of Peptide and Protein Research* **1995**, *45* (5), 488–496. https://doi.org/10.1111/j.1399-3011.1995.tb01065.x.

LC-MS analysis

Ac-Lys(N_3)-Lys(N_3)-Lys(N_3)-Lys(N_3)-Lys(N_3)-Lys(N_3)-TEG-Asp-Glu-Val-Ser-Gly-Leu-Glu-Gln-Leu-Glu-Ser-Ile-Ile-Asn-Phe-Glu-Lys-Leu-Ala-Ala-Ala-Ala-Ala-Lys(sCy5)-NH_2 (19)

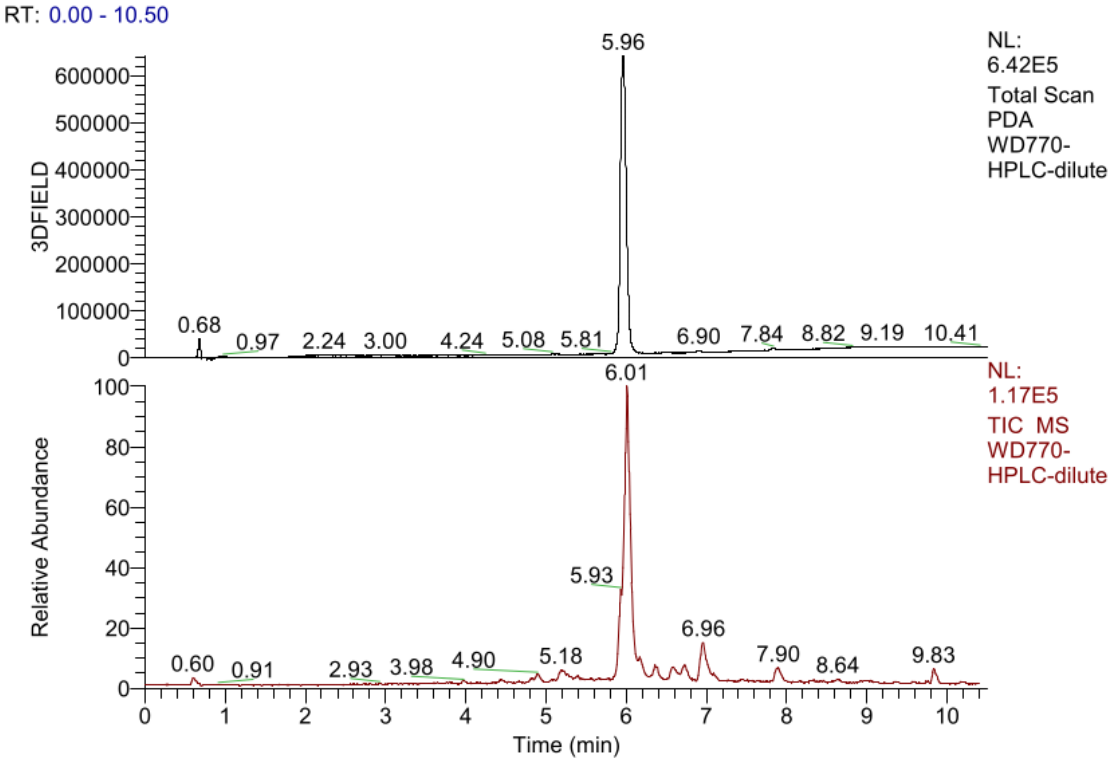

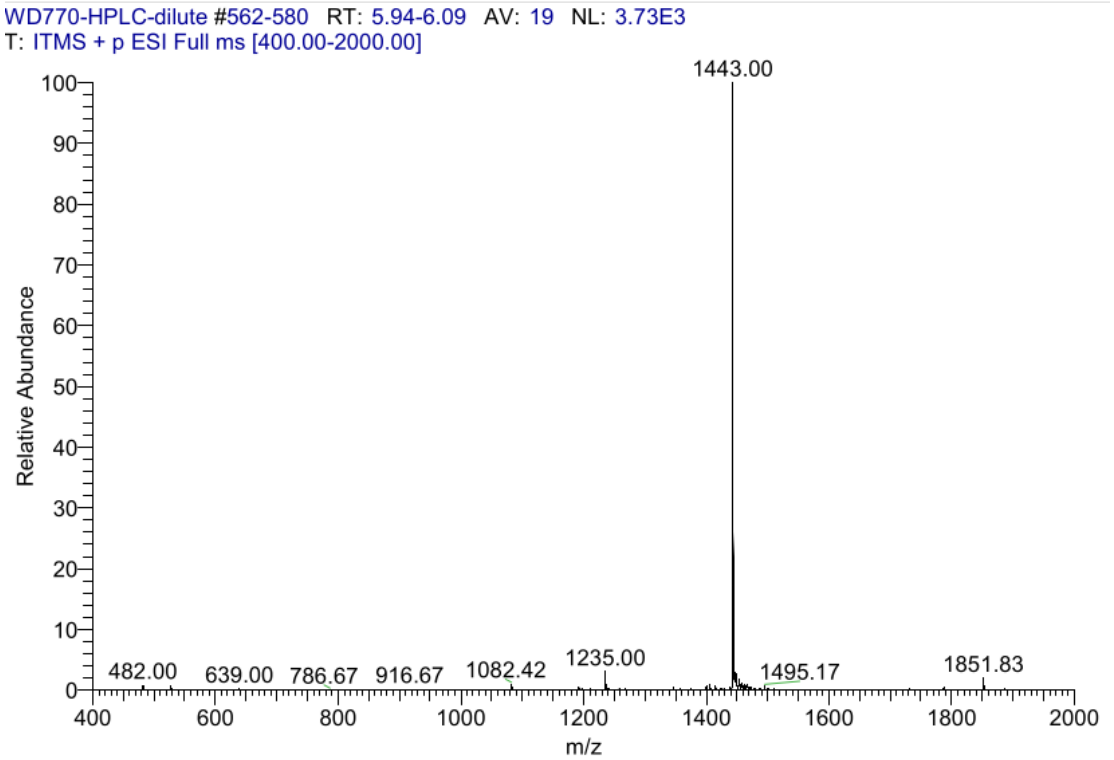

Ac-Lys(N_3)-Gly-Lys(N_3)-TEG-Asp-Glu-Val-Ser-Gly-Leu-Glu-Gln-Leu-Glu-Ser-Ile-Ile-Asn-Phe-Glu-Lys-Leu-Ala-Ala-Ala-Ala-Ala-Lys(sCy5)-NH_2 (21)

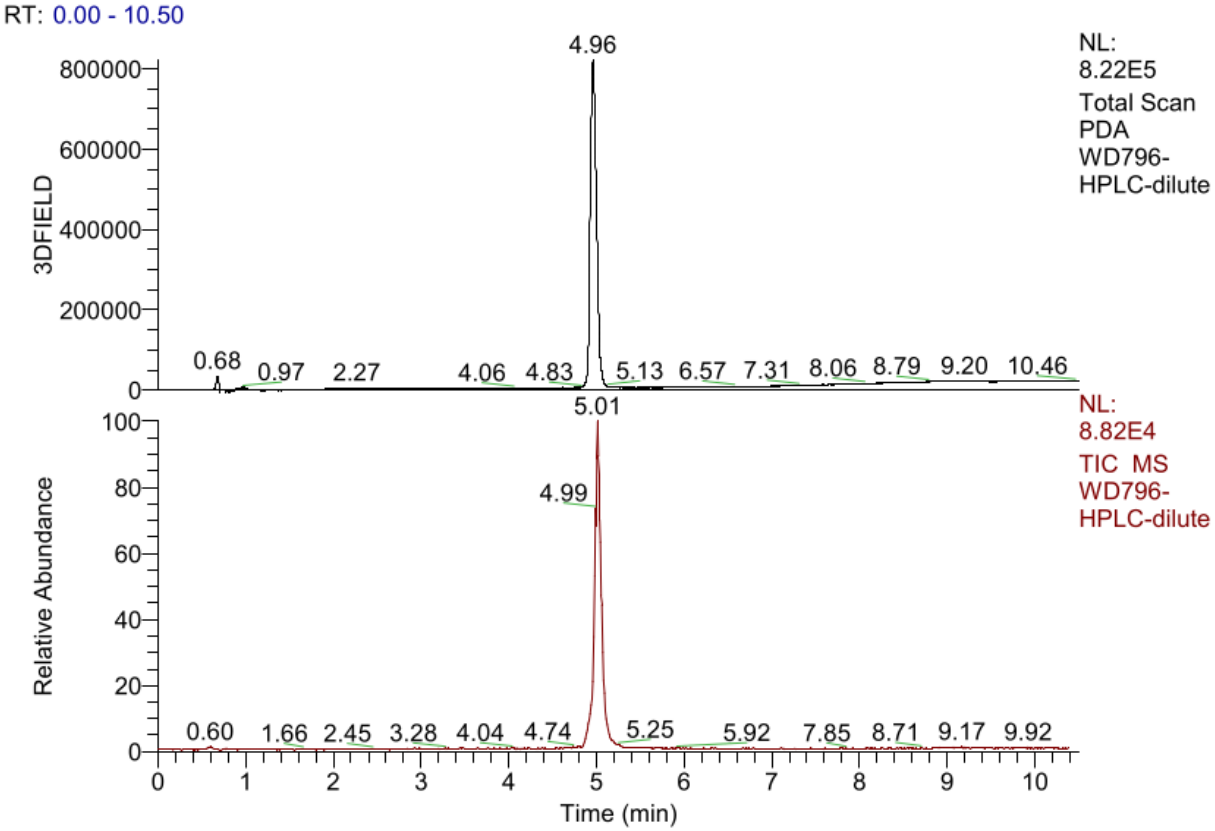

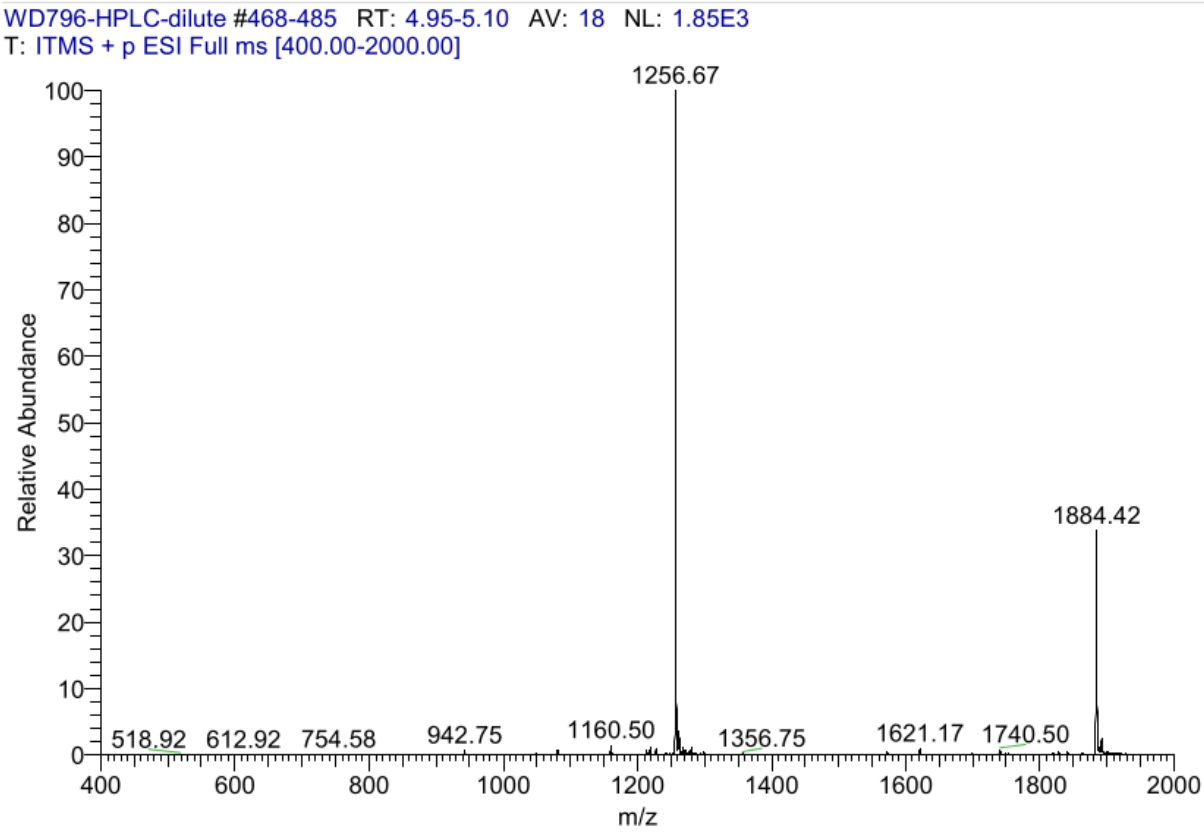

Ac-Lys(N_3)-TEG-Asp-Glu-Val-Ser-Gly-Leu-Glu-Gln-Leu-Glu-Ser-Ile-Ile-Asn-Phe-Glu-Lys-Leu-Ala-Ala-Ala-Ala-Ala-Lys(sCy5)-NH_2 (23)

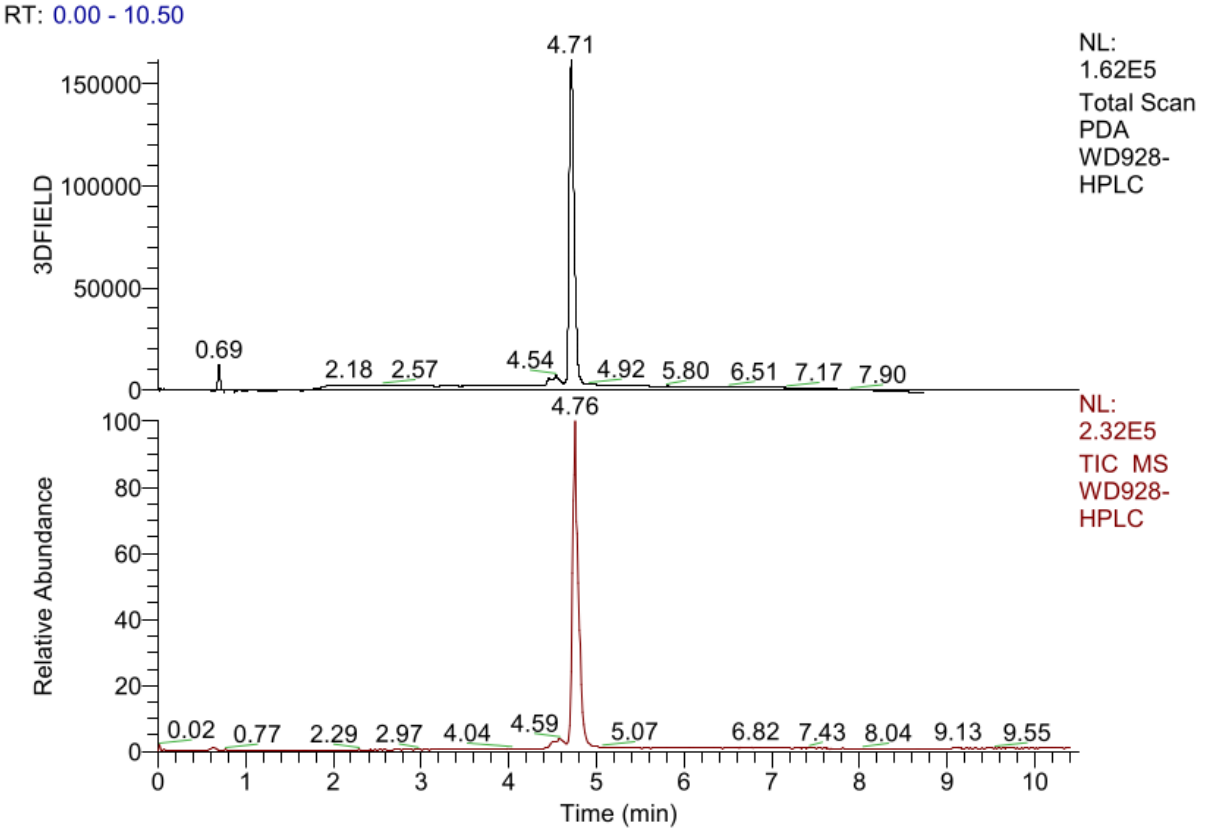

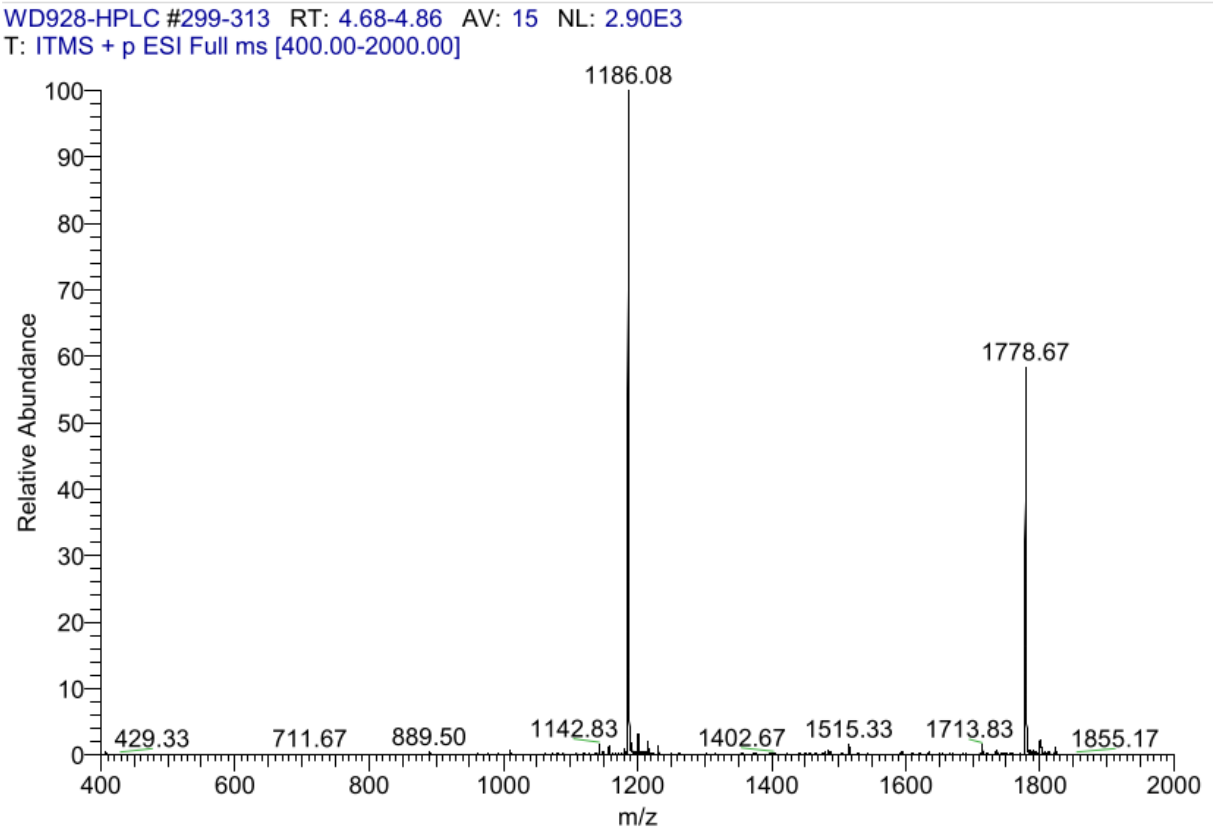

Ac-Lys(Man)-Lys(Man)-Lys(Man)-Lys(Man)-Lys(Man)-Lys(Man)-TEG-Asp-Glu-Val-Ser-Gly-Leu-Glu-Gln-Leu-Glu-Ser-Ile-Ile-Asn-Phe-Glu-Lys-Leu-Ala-Ala-Ala-Ala-Ala-Lys(sCy5)-NH_2 (3)

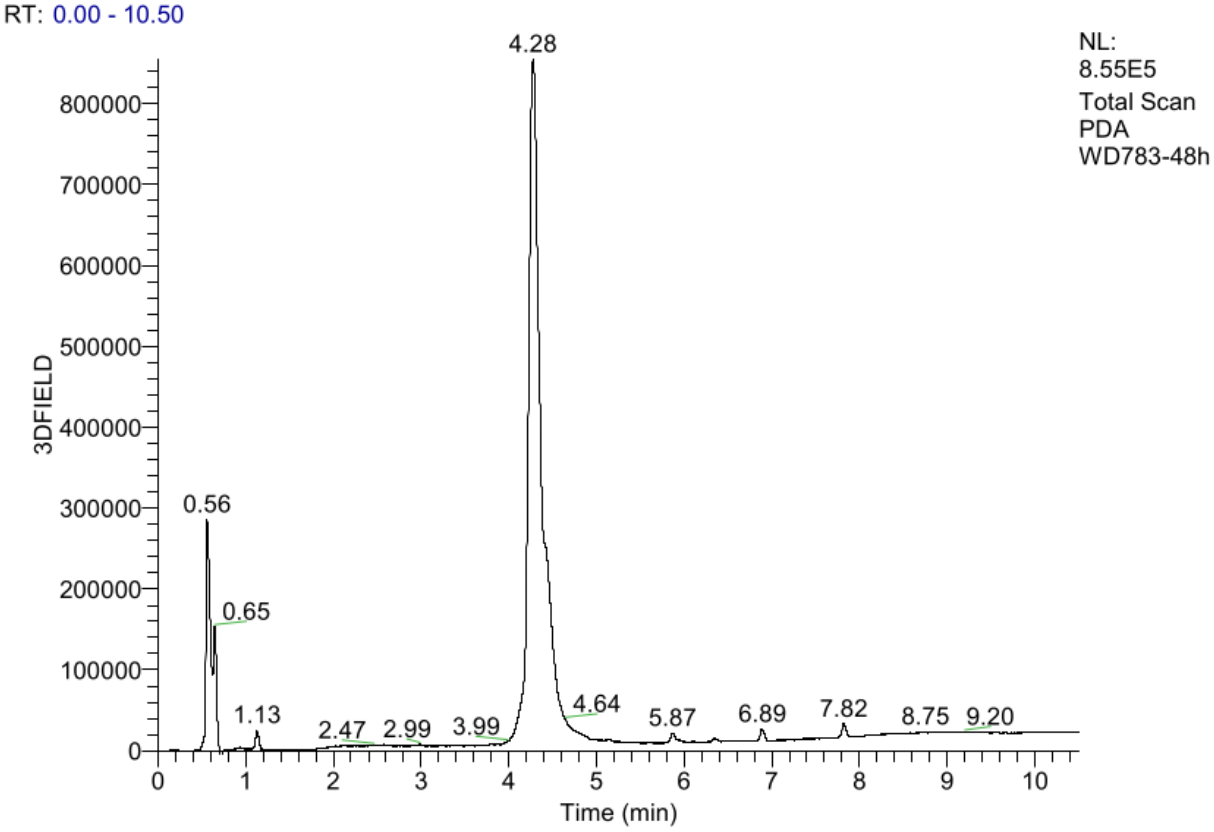

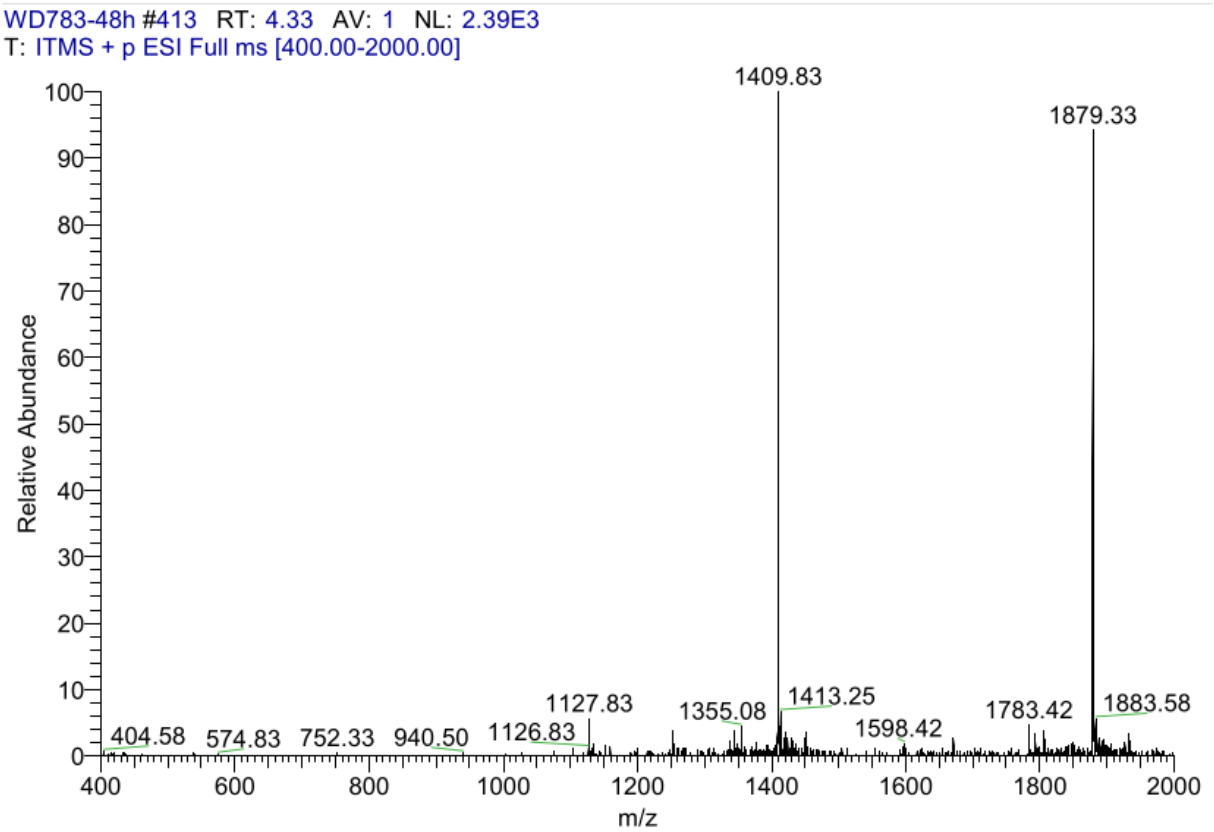

Ac-Lys(triMan)-Lys(triMan)-Lys(triMan)-Lys(triMan)-Lys(triMan)-Lys(triMan)-TEG-Asp-Glu-Val-Ser-Gly-Leu-Glu-Gln-Leu-Glu-Ser-Ile-Ile-Asn-Phe-Glu-Lys-Leu-Ala-Ala-Ala-Ala-Ala-Lys(sCy5)-NH_2 (6)

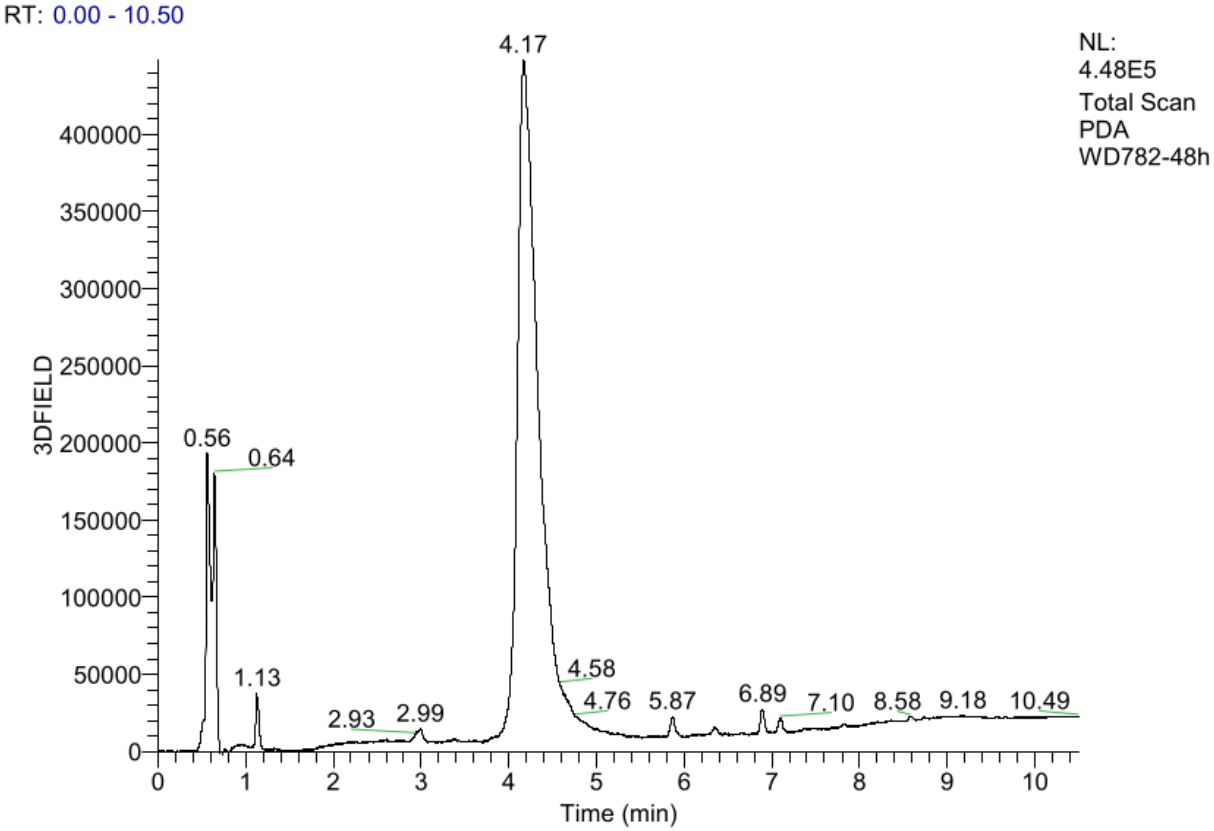

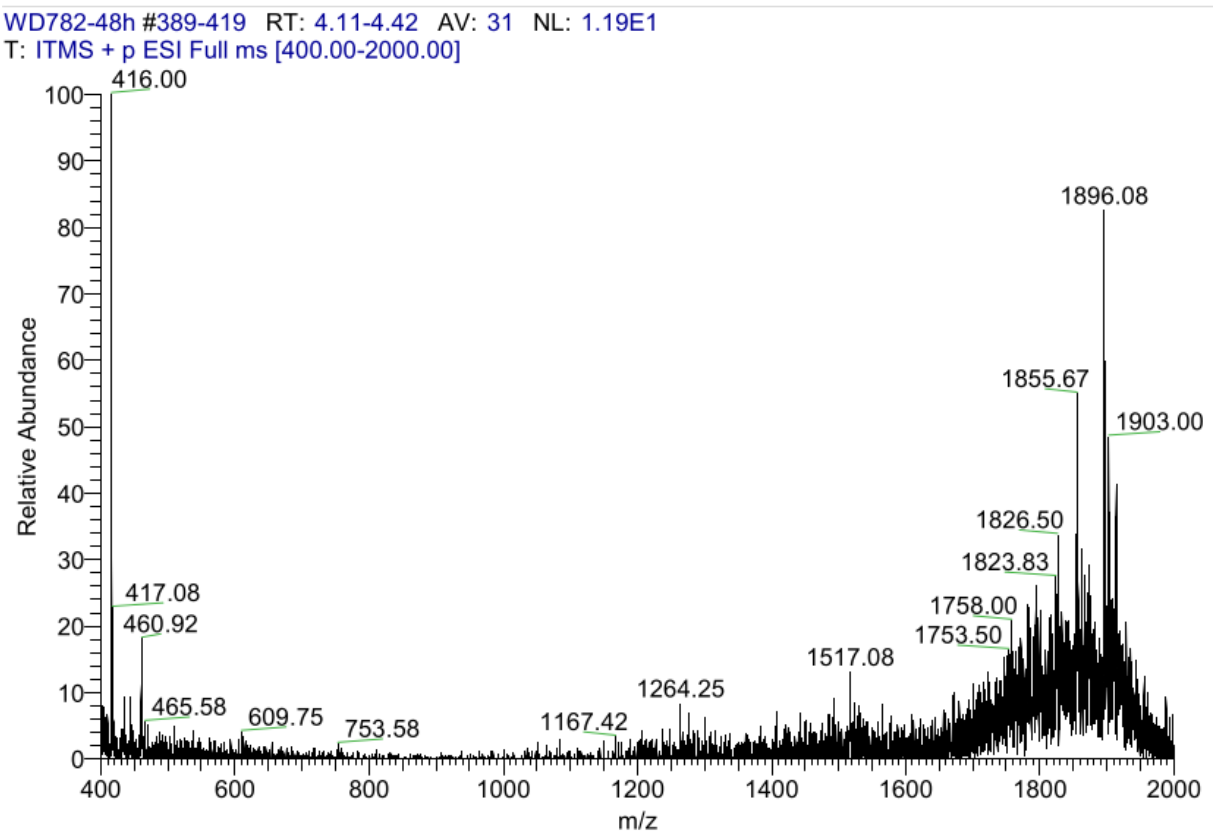

Ac-Lys(Man)-Gly-Lys(Man)-TEG-Asp-Glu-Val-Ser-Gly-Leu-Glu-Gln-Leu-Glu-Ser-Ile-Ile-Asn-Phe-Glu-Lys-Leu-Ala-Ala-Ala-Ala-Ala-Lys(sCy5)-NH_2 (2)

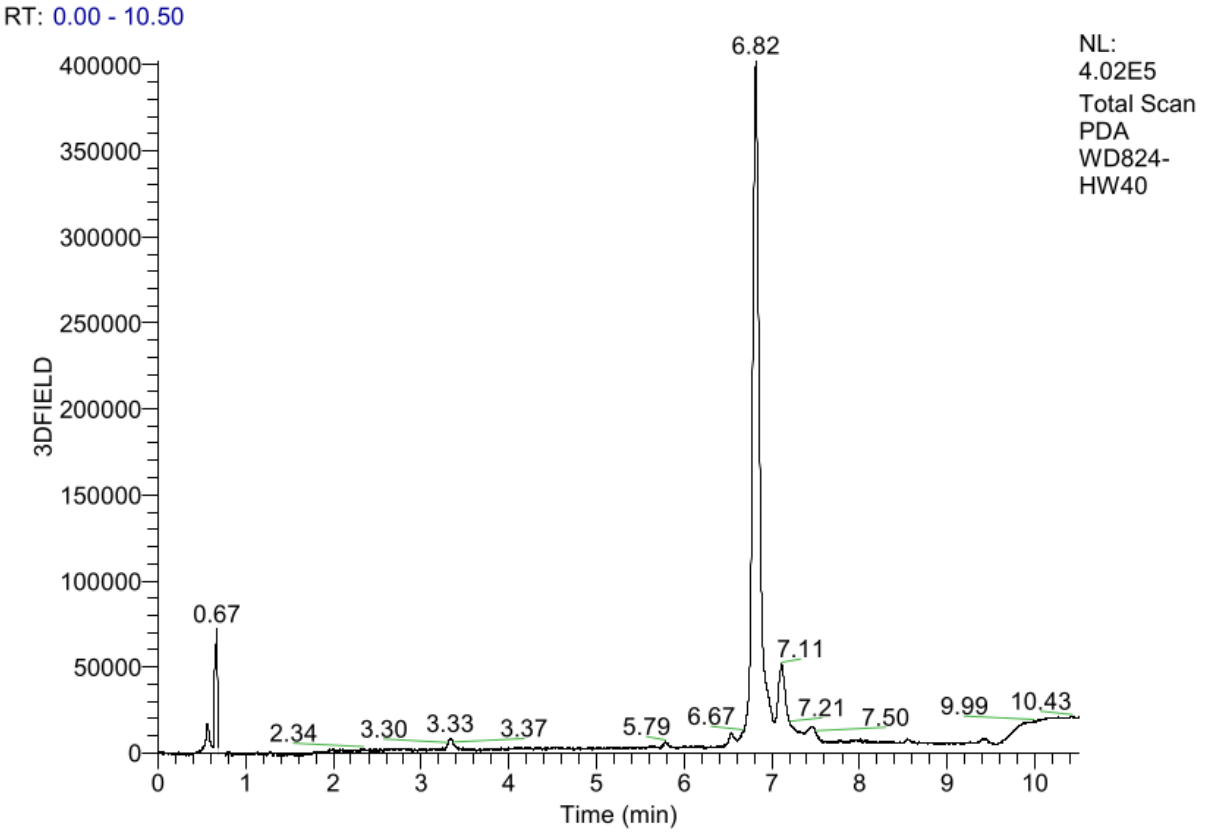

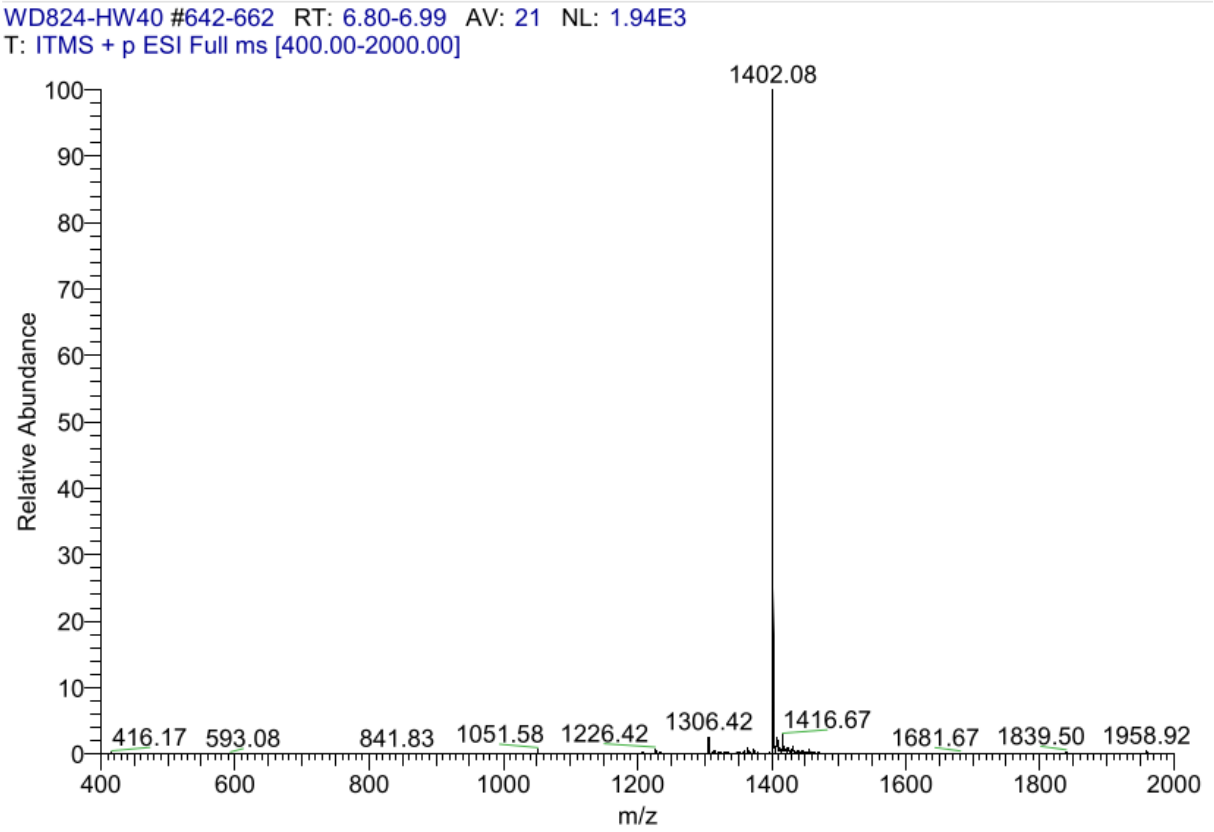

Ac-Lys(triMan)-Gly-Lys(triMan)-TEG-Asp-Glu-Val-Ser-Gly-Leu-Glu-Gln-Leu-Glu-Ser-Ile-Ile-Asn-Phe-Glu-Lys-Leu-Ala-Ala-Ala-Ala-Ala-Lys(sCy5)-NH_2 (5)

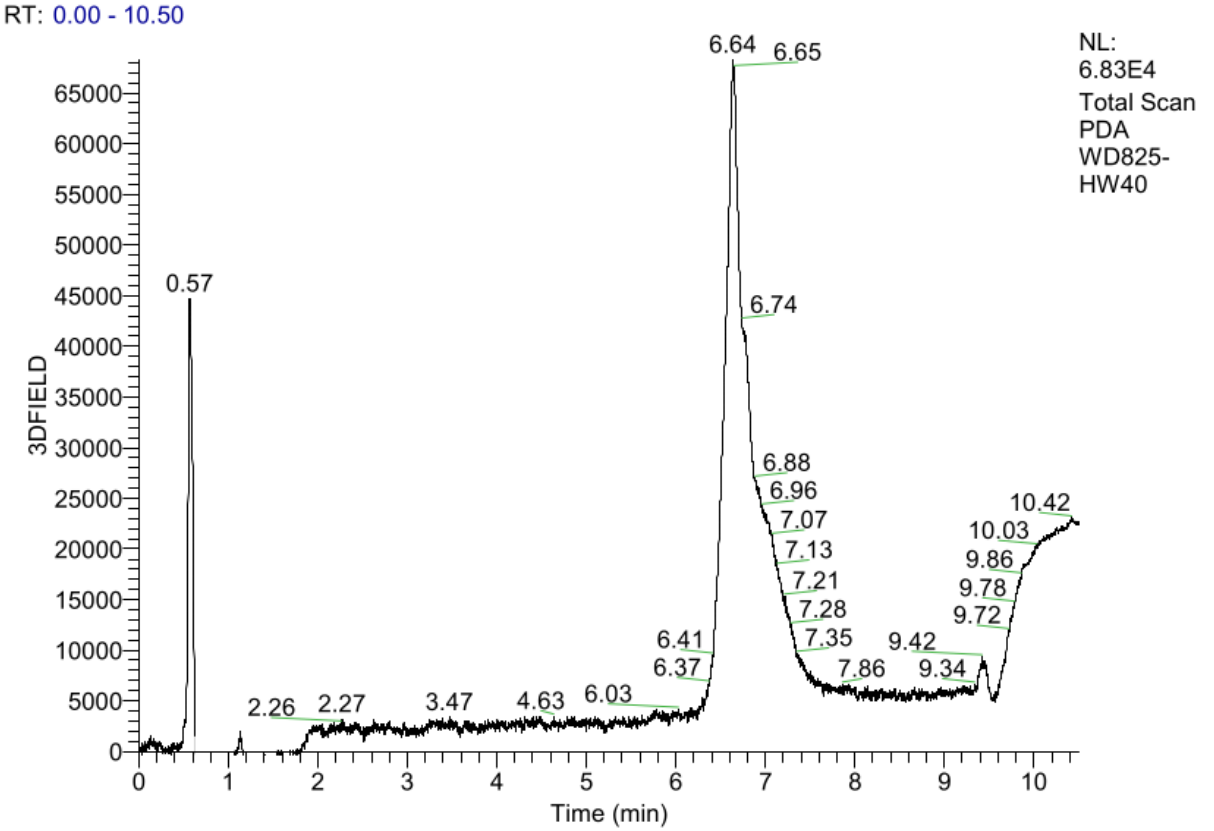

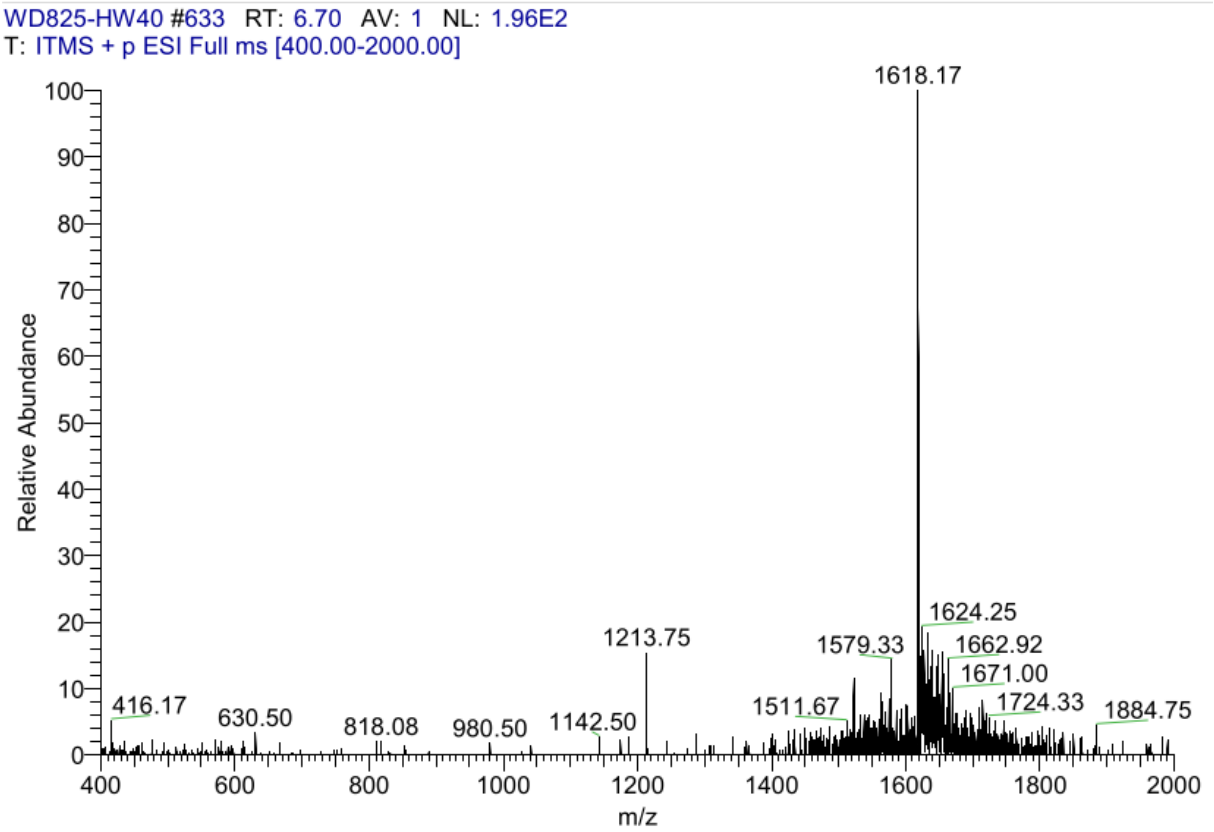

Ac-Lys(Man)-TEG-Asp-Glu-Val-Ser-Gly-Leu-Glu-Gln-Leu-Glu-Ser-Ile-Ile-Asn-Phe-Glu-Lys-Leu-Ala-Ala-Ala-Ala-Ala-Lys(sCy5)-NH$_2$ (1)

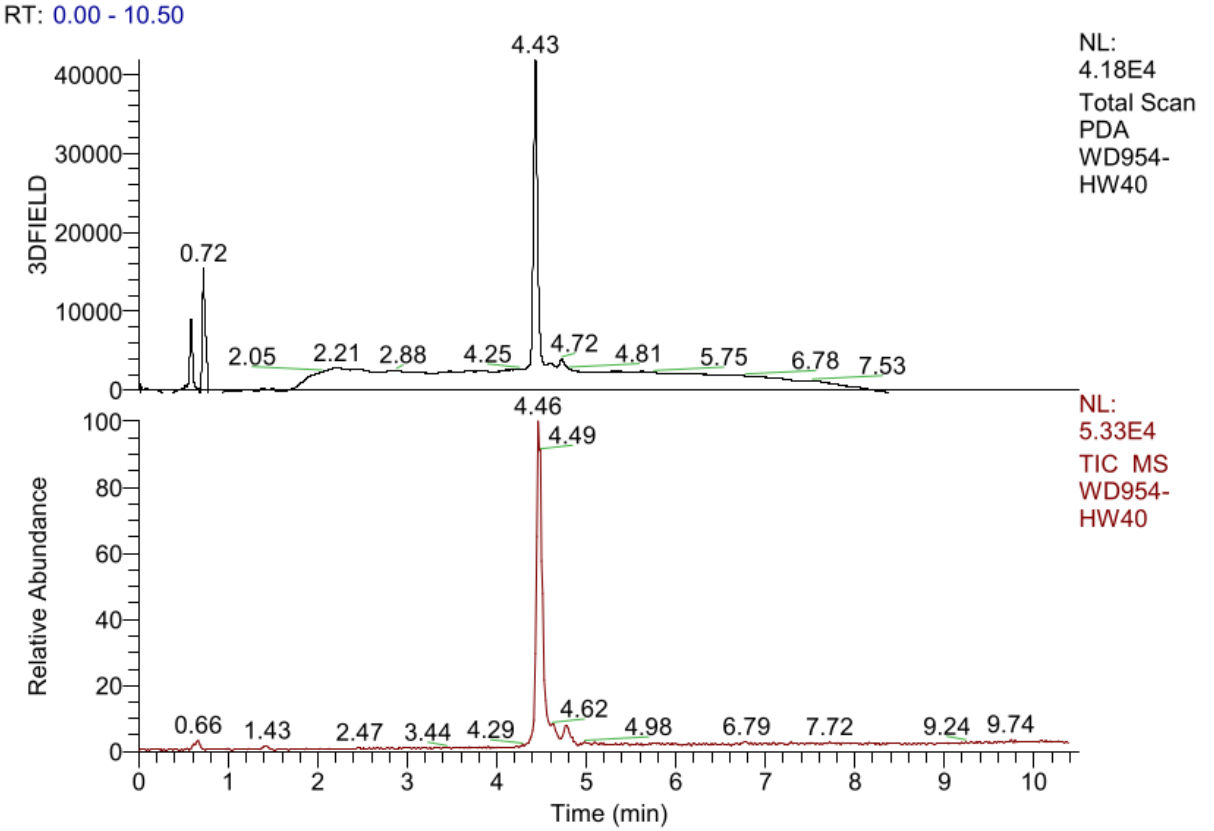

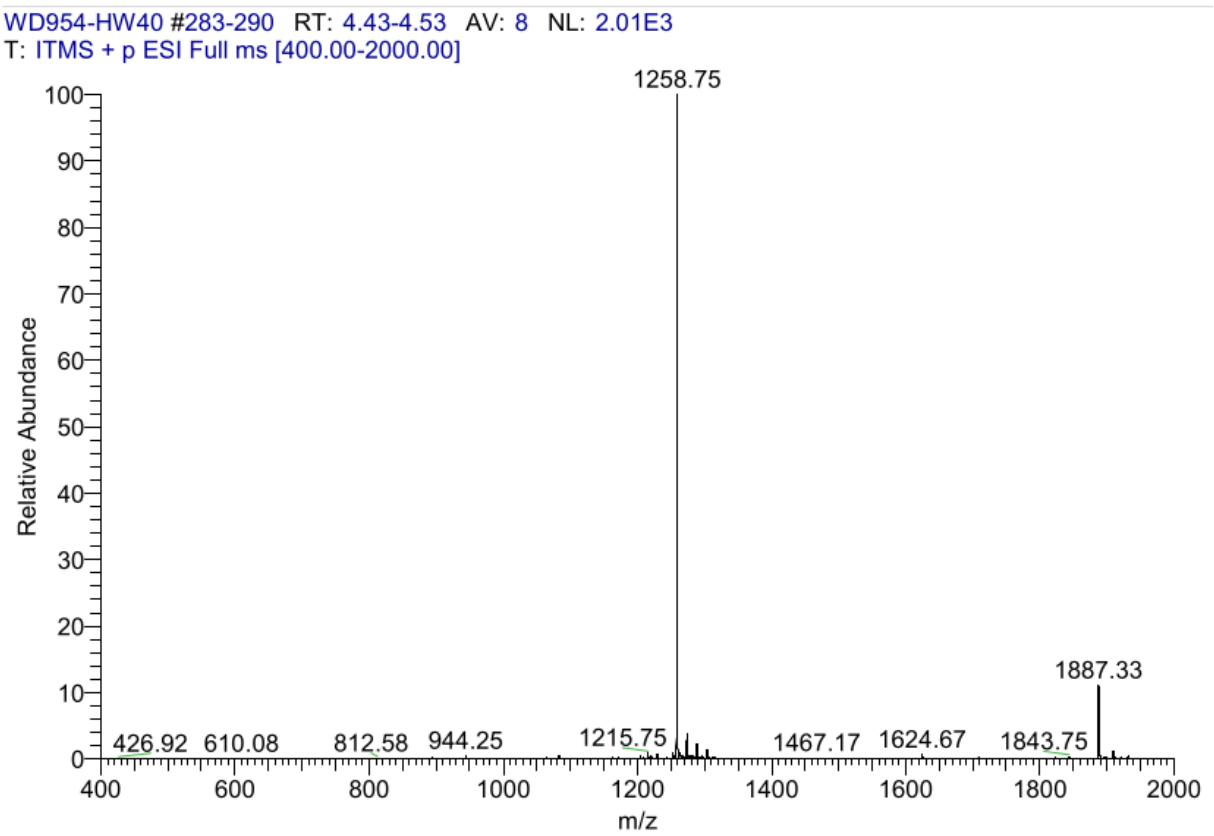
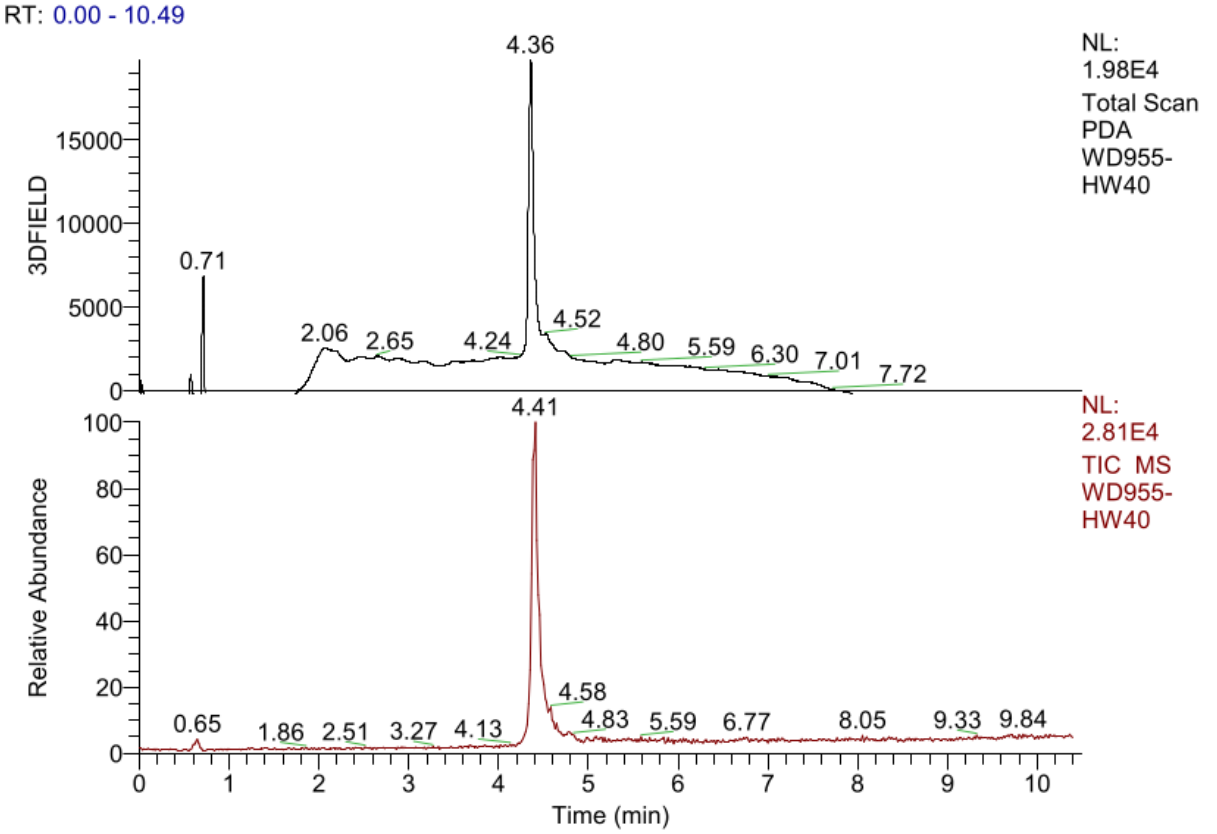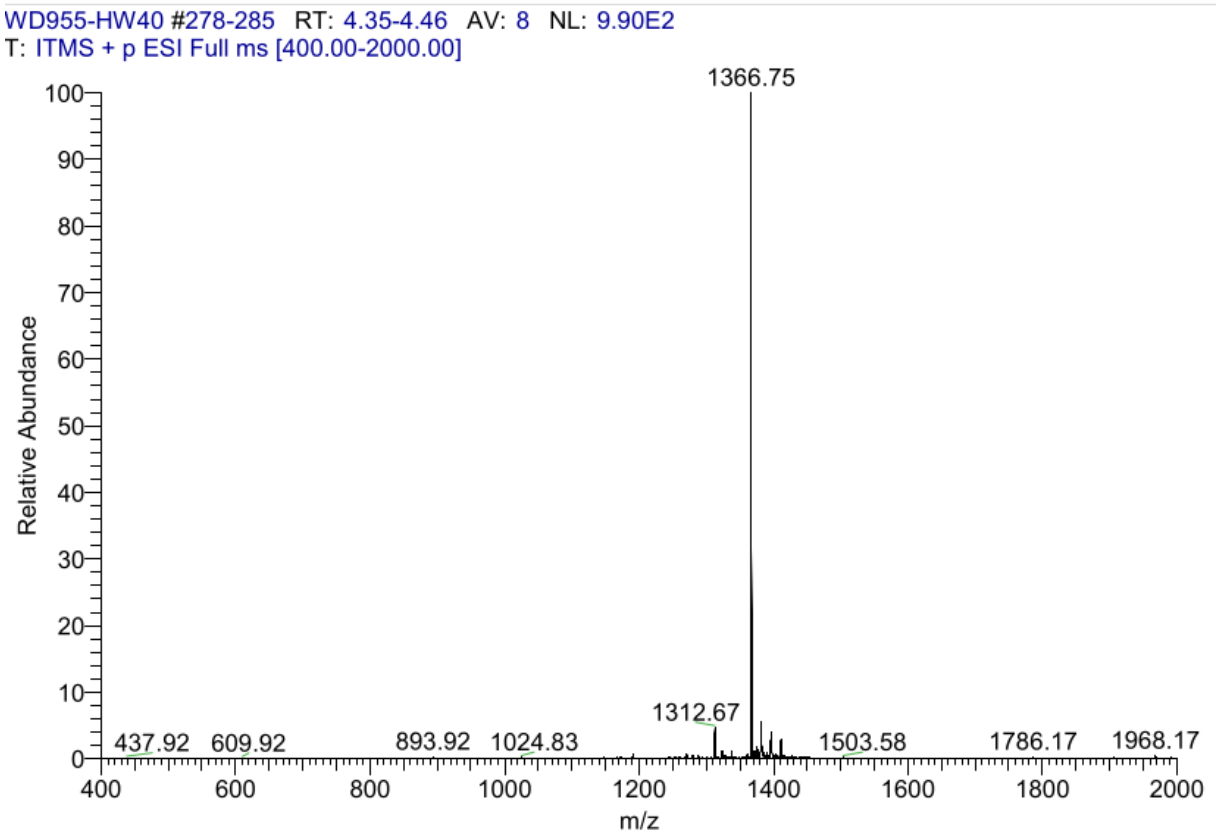
Ac-Lys(triMan)-TEG-Asp-Glu-Val-Ser-Gly-Leu-Glu-Gln-Leu-Glu-Ser-Ile-Ile-Asn-Phe-Glu-Lys-Leu-Ala-Ala-Ala-Ala-Ala-Lys(sCy5)-NH_2 (4)